PoliTO Springer Series

Nosherwan Shoaib

Vector Network Analyzer (VNA) Measurements and Uncertainty Assessment

POLITECNICO
DI TORINO

Springer

PoliTO Springer Series

Springer, in cooperation with Politecnico di Torino, publishes the PoliTO Springer Series. This co-branded series of publications includes works by authors and volume editors mainly affiliated with Politecnico di Torino and covers academic and professional topics in the following areas: Mathematics and Statistics, Chemistry and Physical Sciences, Computer Science, All fields of Engineering. Interdisciplinary contributions combining the above areas are also welcome. The series will consist of lecture notes, research monographs, and briefs. Lectures notes are meant to provide quick information on research advances and may be based e.g. on summer schools or intensive courses on topics of current research, while SpringerBriefs are intended as concise summaries of cutting-edge research and its practical applications. The PoliTO Springer Series will promote international authorship, and addresses a global readership of scholars, students, researchers, professionals and policymakers.

More information about this series at http://www.springer.com/series/13890

Nosherwan Shoaib

Vector Network Analyzer (VNA) Measurements and Uncertainty Assessment

POLITECNICO
DI TORINO

Springer

Nosherwan Shoaib
The Petroleum Institute
Abu Dhabi
United Arab Emirates

ISSN 2509-6796 ISSN 2509-7024 (electronic)
PoliTO Springer Series
ISBN 978-3-319-44771-1 ISBN 978-3-319-44772-8 (eBook)
DOI 10.1007/978-3-319-44772-8

Library of Congress Control Number: 2016949096

Printed on acid-free paper

This Springer imprint is published by Springer Nature
The registered company is Springer International Publishing AG
The registered company address is: Gewerbestrasse 11, 6330 Cham, Switzerland

The most important aspect of any phenomenon from a mathematical point of view is that of a measurable quantity. I shall therefore consider electrical phenomena chiefly with a view to their measurement, describing the methods of measurement, and defining the standards on which they depend.

—James Clerk Maxwell

To my beloved parents

Preface

During the last decade, the industrial and scientific applications are increasingly using the millimeter- and submillimeter-wave part of the electromagnetic spectrum. Some applications include the radar and remote sensing, climate research, wireless communication, security scanners and even medical diagnosis systems. This is due to the higher data rates, circuit miniaturization and higher spatial resolution properties of the high-frequency bands. The development of reliable, high-quality and safer products at these frequencies is highly dependent on the availability of the precise and reliable network analysis. Therefore, along with performing measurements, the associated uncertainty evaluation is also very important.

The vector network analyzers (VNAs) are commonly used for network analysis with great accuracy and precision. VNAs are complex and versatile instruments employed to characterize active and passive networks used in communication technologies. The network characterization is defined in terms of scattering parameters (S-parameters). The S-parameters are ratios of wave quantities which provide information about reflection and transmission characteristics of the device under test (DUT). The VNA measurements are associated with different sources of errors; mainly classified as systematic, random and drift errors. During a VNA calibration procedure, the systematic errors are characterized and most of them are mathematically removed afterwards. The other sources of errors can possibly be minimized; however, they affect the S-parameter measurements and become different sources of uncertainty associated with the measurements. Therefore, the uncertainty analysis is also an integral part while doing measurements with VNAs.

The aim of the book is to describe the VNA measurements and uncertainty assessments particularly in waveguide test-set environments, in order to establish the measurement traceability to the International System of Units (SI) for accurate and reliable characterization of communication networks. The frequency of interest ranges from few a MHz up to Terahertz frequency band. A fully analytical approach for uncertainty evaluation is discussed. The uncertainty sources considered are the definitions of the calibration standards, VNA noise, repeatability and drift. The interaction and the linear propagation of different uncertainty sources to compute

the final uncertainties associated with the measurements are also shown. The dimensional characterization of standards is also the part of the discussion.

In the Chap. 1, a general introduction to the VNA measurements and uncertainty assessment is presented. The different measurement errors, calibration standards and the calibration techniques are also described. A brief description is also provided for the classification of the uncertainty components and the S-parameter uncertainty representation.

Chapter 2 basically deals with the S-parameter measurements and uncertainty evaluation at millimeter frequencies. The analytical treatment of uncertainty propagation is discussed. The uncertainty propagation flowchart is also presented which provides information about the interaction of different uncertainty sources associated with the VNA measurements. To elaborate the matter, the S-parameter measurements and uncertainty evaluation at millimeter frequencies (50–110 GHz) are presented. The electromagnetic computations based on mechanical characterization of the waveguide shim standards are also the part of the discussion. A compatibility assessment between different S-parameter data is also carried out.

In the Chap. 3, a comparison of different S-parameter calibration techniques at millimeter frequencies (75–110 GHz) is described. All the calibration standards are mechanically measured and different calibration techniques are used for tracing S-parameter measurements to the *SI*. The aim of this comparison is to analyze the efficiency of two different VNA calibration techniques in terms of S-parameter measurements and related uncertainty.

In the Chap. 4, the connection repeatability investigation of a waveguide VNA in WR05 (140–220 GHz) is presented. The connection repeatability investigation is important to analyze the variability of the repeated measurements and flange alignment mechanisms. In particular, this investigation is very important from metrological point of view at these frequencies because of the very small dimensions of the waveguide apertures.

Finally, in the Chap. 5, the suitable verification artefacts to check the performance of the VNAs, in particular the linearity, including their applicability to coaxial and waveguide systems are described. The waveguide verification standards considered for analysis are: WR-05 (140–220 GHz) and WR-03 (220–325 GHz) cross-guides and a custom-made WR-03 (220–325 GHz) circular iris section. Moreover, the analysis, design and fabrication of a novel type N coaxial verication standard architecture (DC-18 GHz) based on an air-line are presented.

Abu Dhabi, United Arab Emirates Nosherwan Shoaib

Acknowledgments

The contents of this book are based on my research activities carried out at Politecnico di Torino, Italy, Istituto Nazionale di Ricerca Metrologica—INRiM, Italy, National Physical Laboratory—NPL, UK and Physikalisch-Technische Bundesanstalt—PTB, Germany. My gratitude goes to the people from these institutions who have motivated me and provided useful suggestions that made it possible for me to write this book. In particular, I am grateful to Prof. Andrea Ferrero of Politecnico di Torino, Dr. Luciano Brunetti, Dr. Marco Sellone and Dr. Luca Oberto of INRiM, Prof. Nick Ridler and Mr. Martin Salter of NPL and Dr. Rolf Judaschke and Dr. Karsten Kuhlmann of PTB. I also would like to thank my family for inspiring me and supporting me throughout and dedicated this book to them.

Contents

Chapter 1
General Introduction

Abstract A vector network analyzer (VNA) is a complex and versatile instrument that is used in the field of radio frequency (RF) engineering for accurate and precise measurements. The goal of this chapter is to review briefly the VNA architecture and the measurement errors. The VNA calibration standards and the calibration techniques will also be discussed. This chapter will conclude with an overview of the measurement uncertainty.

1.1 Introduction

In radio frequency (RF) engineering, the network analysis is one of the most common and important tasks. The network analyzer is an instrument, widely used for this purpose, that performs measurements of the networks with great efficiency and accuracy. The networks can be amplifiers, filters or some complex devices that are used in satellite communications. The network analyzer finds applications in research and development as well as in industrial production. The measurements from network analyzer can be used to study the material properties. Applying the imaging and signal processing techniques to the data obtained from this instrument provides information about material defects. It is also widely used to perform antenna measurements in Radar system [1].

The sinusoidal signal generated from the network analyzer is applied to the device under test (DUT). The instrument then measures the response of the DUT. The signal coming back from DUT to network analyzer has a different amplitude and phase as compared to the signal that goes to the DUT. These wave quantities are the signals used to characterize the DUTs. The network analyzers are classified into two types:

- Scalar network analyzer
- Vector network analyzer (VNA)

The scalar network analyzer measures only the amplitude difference between the wave incident to the DUT and the wave reflected from the DUT. On the other hand, the VNA measures both amplitude and phase of the incident and the reflected waves. So, the VNA requires more complex implementation but has higher accuracy and

N. Shoaib, *Vector Network Analyzer (VNA) Measurements and Uncertainty Assessment*, PoliTO Springer Series, DOI 10.1007/978-3-319-44772-8_1

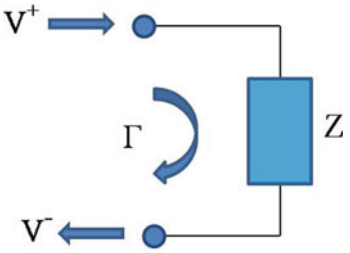

Fig. 1.1 One-port network

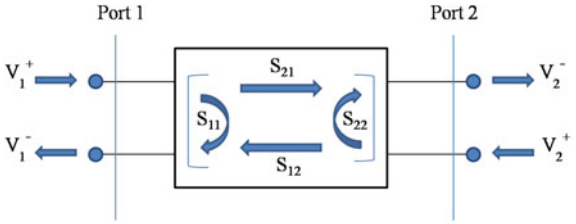

Fig. 1.2 Two-port network

precision. The frequency domain data obtained from the VNA can be transformed into the time domain for further analysis.

VNA can be used to characterize one-, two- or multi-port networks. A one port network is shown in Fig. 1.1, where V^+ is the amplitude of the incident voltage wave and V^- is the amplitude of the reflected voltage wave. The ratio between the incident voltage wave V^+ that propagates from the VNA to the DUT to the reflected voltage wave V^- from DUT to the VNA is called reflection coefficient Γ; where Z is the impedance of the network. This Γ measurement provides the information about the response of the network.

$$\Gamma = \frac{V^-}{V^+} \tag{1.1}$$

In a two-port network, as the one shown in Fig. 1.2, there also exist forward and reverse transmissions besides the reflections. These quantities can be expressed in terms of scattering parameters (S-parameters) [1]. The S-parameters are defined as the ratios of the reflected and incident wave quantities. In case of two-port network, the four S-parameters S_{11}, S_{21}, S_{12} and S_{22} are required to completely characterize the network. The S_{11} and S_{22} are the input and the output reflection coefficients at port 1 and port 2 respectively. While the S_{21} and S_{12} represent the forward and reverse transmission coefficients respectively.

The S-parameters can be written in matrix form as follows:

$$\begin{bmatrix} V_1{}^- \\ V_2{}^- \end{bmatrix} = \begin{bmatrix} S_{11} & S_{12} \\ S_{21} & S_{22} \end{bmatrix} \begin{bmatrix} V_1{}^+ \\ V_2{}^+ \end{bmatrix}, \tag{1.2}$$

where V_1^- and V_2^- are the reflected waves and V_1^+ and V_2^+ are the incident waves at port 1 and 2. In a more general form, these S-parameters can be written as:

$$S_{mn} = \left.\frac{V_m^-}{V_n^+}\right|_{V^+_{m\neq n}=0} \tag{1.3}$$

Equation 1.3 implies that the S-parameters are the ratios of the reflected and incident wave measurements, while terminating the other port on reference impedance. The S-parameters are preferred and easier to use as compare to Z- or Y-parameters at high frequencies. This is due to the fact that the S-parameters use matched terminations while characterizing the DUT, while Z- and Y-parameters are based on open and short circuit terminations. The matched terminations are much easier to use at high frequencies as compare to open and short circuit terminations [2].

1.2 VNA Architecture

The basic model of the VNA is shown in Fig. 1.3. The RF source generates the signal which is applied to the DUT and the DUT response is measured. The RF switch used with the source passes the RF signal to one of the test ports. The directional

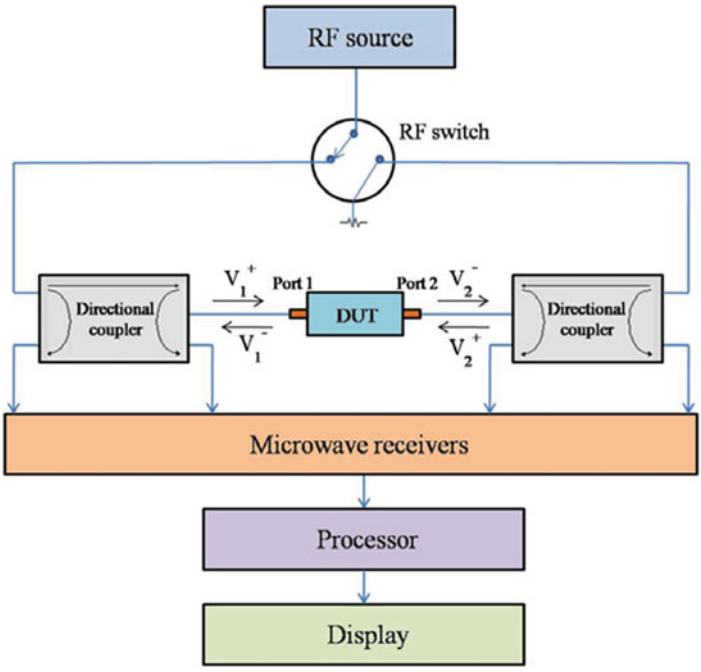

Fig. 1.3 Block diagram of a VNA

couplers are used for signal separation. They measure the incident signal to be used as a reference for computing the wave quantity ratios and separate the incident signals (V^+) and the reflected signals (V^-) at the input of the DUT. The microwave receivers are used to down convert the RF signal to a lower intermediate frequency (IF). Some VNAs have four receivers and some have three. The magnitude and phase information from the IF signal is extracted using the analog to digital converter (ADC) and the digital signal processing (DSP). Afterwards, the error correction is performed and the measurement data is displayed [1].

The S-parameter measurements with the VNA contain measurement errors due to imperfections in the VNA and test setup, noise and drift. Some measurement errors are corrected via calibration procedure while the residual errors come up as the source of uncertainty associated with the measurements. The next few sections will elaborate the VNA measurements and the associated uncertainties.

1.3 VNA Measurements

The accuracy of the measurements can be improved by knowing how the errors occur during the measurements and how to correct them. The errors that are not corrected come as a source of uncertainty associated with the measurements.

1.3.1 Measurement Errors

The VNA measurement errors are classified into three main groups:

- Systematic Errors
- Random Errors
- Drift Errors

Systematic Errors

The imperfections in the VNA and test setup are the main cause of systematic errors. These errors are repeatable, therefore they can be predicted. They are also time invariant. Most of the systematic errors can be characterized using the calibration process and then removed mathematically afterwards. Both reflection and transmission measurements generate systematic errors. The systematic errors generated during the transmission measurements are the following [1, 3]:

- **Isolation error**: is the signal leakage, also called crosstalk;
- **Load match error**: is due to some signal reflected off of the port during transmission measurements;
- **Transmission tracking error**: is due to the non identical frequency response of the receivers during transmission measurements.

The systematic errors generated during the reflection measurements are categorized as follows:

- **Directivity error**: is due to the leakage of directional coupler;
- **Source match error**: is due to the multiple internal reflections between the analyzer and the DUT;
- **Reflection tracking error**: is due to the non identical frequency response of the receivers during reflection measurements.

Using a particular combination of calibration standards, the calibration procedure characterizes these systematic errors and removes them mathematically during measurements. However, they cannot be removed completely due to calibration standards imperfection, connector interface and instrumentation.

Random Errors

Random errors are unpredictable by nature. Therefore, these errors can not be removed by calibration process. However, they can be minimized to improve the measurement accuracy. Following are the main sources of random noise [3]:

- **Low-level noise**: or background noise is caused by the measurement channel;
- **High-level noise or jitter noise**: is due to the phase noise of the local oscillator (LO) source;
- **Switch Repeatability errors**: are due to the mechanical RF switches contacts;
- **Connector repeatability errors**: are due to the connector wear.

The random errors can be minimized by using a narrow IF bandwidth, increasing source power to the DUT, avoiding the switching attenuator settings and preventing the connector damage.

Drift Errors

These errors are due to the performance change of the VNA after calibration. These errors are mostly caused by the following reasons [3]:

- Thermal expansion characteristics of interconnecting cables
- Conversion stability of the microwave frequency converter

These errors can be removed by re-calibrating the instrument. Also, the stable ambient temperature minimizes the drift.

1.3.2 Calibration Standards

The calibration procedure requires particular combination of one and two port standards. The one port standards include Short, Open, Load and Sliding Load. The Line or a reciprocal network can be used as two port calibration standards. The calibration standards types are available in coaxial, waveguide and on-wafer environments.

Here, both coaxial and waveguide standards are discussed. However, in this book, we will mainly focus on waveguide standards except in Chap. 5 where the coaxial verification standards are also discussed. A brief description of one and two port calibration standards will be given in the following.

Short

This one port standard ideally has reflection coefficient modulus $|\Gamma|$ equal to 1. In coaxial design, however, due to mechanical reasons, there exists an offset length l between the reference plane and the short plane. Therefore, Γ is dependent on l. Mathematically, Γ at the reference plane of the offset short standard can be written as follows [1]:

$$\Gamma = -e^{-2(\alpha+j\beta)l} \tag{1.4}$$

where α is the attenuation constant expressed in nepers per metre (Np/m) and β is the phase constant expressed in radians per metre (rad/m). The symbol α represents the attenuation of the electromagnetic wave propagating through the medium per unit distance, while β represents the phase change per metre as wave travels along the path. Since the loss due to offset length l is negligible i.e. $\alpha = 0$, therefore, the Eq. 1.4 reduces to:

$$\Gamma = -e^{-j4\pi l/\lambda} \tag{1.5}$$

where

$$\beta = 2\pi/\lambda \tag{1.6}$$

and

$$\lambda = c/f \tag{1.7}$$

where c = 299792458 m/s is the speed of light in vacuum and f is the frequency of operation.

In some cases, Γ for the short standard can be modeled in terms of parasitic inductances [1]. The frequency dependent parasitic inductance L(f) can be approximated using a third order series expansion as shown below:

$$L(f) = L_0 + L_1 f + L_2 f^2 + L_3 f^3 \tag{1.8}$$

Now Γ can be written as:

$$\Gamma = \frac{j2\pi f L(f) - Z_0}{j2\pi f L(f) + Z_0} e^{-j4\pi l/\lambda} \tag{1.9}$$

In case of waveguide systems, the short standard can be a conductive plate mounted on the waveguide flange of the test port which implies that the waveguide short standard has zero offset length l. For offset short waveguide standard, the reflection coefficient is dependent on the offset length. Also, the wavelength in waveguides is frequency dependent due to the dispersive nature of the waveguides. For hollow pipe

rectangular and circular waveguides, the dominant transverse electromagnetic (TE) mode is TE_{10} because this mode has lowest cutoff frequency. The cutoff frequency f_c for TE_{10} mode of an rectangular waveguide with inner dimensions a, b (where a > b) can be written mathematically as [1]:

$$f_c = \frac{c}{2a\sqrt{\epsilon_r \mu_r}} \tag{1.10}$$

where both the relative permittivity ϵ_r and relative permeability μ_r are approximately equal to 1 for air. Similarly, the cutoff wavelength λ_c can be written as:

$$\lambda_c = 2a \tag{1.11}$$

The mathematical formulation for waveguide wavelength λ_w in terms of λ_c will be:

$$\lambda_w = \frac{\lambda}{\sqrt{1 - (\lambda/\lambda_c)^2}} \tag{1.12}$$

Open

For coaxial open standard, a closed design must be used because radiation effects can occur at the open end of the inner conductor. In a closed design, a frequency dependent fringing capacitance is formed at the open end of the inner conductor [1]. The frequency dependence of this fringing capacitance *C(f)* can be approximated using a cubic expression as follows:

$$C(f) = C_0 + C_1 f + C_2 f^2 + C_3 f^3 \tag{1.13}$$

The reflection coefficient Γ for the open standard at the reference plane depends on the fringing capacitance *C(f)* and the offset length *l* from the reference plane to the open end of the inner conductor. Mathematically, it can be written as:

$$\Gamma = \frac{1 - j2\pi f Z_0 C(f)}{1 + j2\pi f Z_0 C(f)} e^{-j4\pi l/\lambda} \tag{1.14}$$

In waveguide systems, the open standard does not exist because of the radiation effects at the open end of the waveguide. Therefore, the offset short with offset length of $\lambda_w/4$ can be used as realization for a waveguide open standard.

Load

The load or match standard has a broadband impedance that must match with the system impedance. Ideally, the assumption for the match standard is $|\Gamma| = 0$. However, recently the network analyzers have the possibility of including the non ideal properties of a match standard.

In waveguide match standard, a cone or pyramid shaped structure is fixed to a waveguide piece closed at one end. This cone or pyramid structure is made of ferrite material that acts as an absorber for the electromagnetic energy.

Reflect

The reflect standard is the one which has the reflection coefficient modulus greater than zero i.e. $|\Gamma| > 0$. It is used in calibration procedure that does not require an exact value of reflection coefficient.

Thru

A direct connection between the two test ports is known as thru standard. If the connectors are of same type and different gender or genderless, then a thru connection has electrical length of 0 mm. However, connectors of same type and same gender require a small line section to make a suitable electrical connection between the test ports. Since the waveguides are genderless, therefore, the thru will be a direct connection between the two waveguide test ports of the same type.

Line

The line is a two port standard that has its characteristics impedance that must be matched as close as possible to the reference impedance. In a calibration procedure that uses both line and thru connection, the electrical length of line and thru must be different. This electrical length difference should avoid $\lambda/2$ and its multiples otherwise calibration procedure will produce singularity and become inconsistent. In order to have a broadband frequency range, a greater number of lines of different lengths can be used.

A line standard is usually a symmetrical i.e. $S_{11} = S_{22}$ and reciprocal network i.e. $S_{21} = S_{12}$. Also, the characteristics impedance of the line standard is matched as close as possible to the reference impedance of the system which means $S_{11} = S_{22} \approx 0$. The transmission coefficient S_{21} of the line standard can be written mathematically as follows:

$$S_{21} = e^{-(\alpha + j\beta)l} \tag{1.15}$$

where l is the length of the line in metres (m).

For coaxial transmission lines, the propagation constants can be defined according to the *Coaxial Calibration Coefficient Model*. In this model, the calibration standards are defined by using a terminated transmission line model for 1-port standards and a transmission line model for 2-port standards. The attenuation constant and the phase constant per unit length can be expressed mathematically as follows [4]:

$$\alpha = \left[\frac{(Offset\ Loss)(Offset\ Delay)}{2(Offset\ Z_0)l}\right]\sqrt{\frac{f}{10^9}} \tag{1.16}$$

$$\beta = \omega\frac{(Offset\ Delay)}{l} + \alpha \tag{1.17}$$

and

$$Offset\ Loss = \frac{c}{\sqrt{\epsilon_r/10^9}}\sqrt{\frac{\pi\mu_0}{\sigma_c}}\left(\frac{1}{\pi d}+\frac{1}{\pi D}\right), \tag{1.18}$$

$$Offset\ Delay = \frac{l\sqrt{\epsilon_r}}{c}, \tag{1.19}$$

$$Offset\ Z_0 = \frac{\mu_0 c}{2\pi\sqrt{\epsilon_r}}\ln\left(\frac{D}{d}\right) \tag{1.20}$$

where
$\omega = 2\pi$f is the angular frequency in radians per seconds (rad/sec),
l is the length of the line in metres (m),
d is the outer diameter of the inner conductor in metres (m),
D is the inner diameter of the outer conductor in metres (m),
$\mu_0 = 4\pi 10^{-7}$ H/m is the permeability of free space in henry per metre,
ϵ_r is the relative dielectric constant,
c = 299792458 m/s is the speed of light in vacuum in metres per sec and
σ_c is the electrical conductivity of the copper material in siemens per metre (S/m).

In the case of rectangular waveguides, the mathematical formulations for attenuation constant and phase constant per unit length, according to *Waveguide Calibration Coefficient Model*, are as follows [4]:

$$\alpha = \frac{(Offset\ Loss)(Offset\ Delay)}{l}\left(\sqrt{\frac{\epsilon_0}{\mu_0}}\right)\sqrt{\frac{f}{f_c}}\left[\frac{1+\frac{2h}{w_e}\left(\frac{f_c}{f}\right)^2}{\sqrt{1-\left(\frac{f_c}{f}\right)^2}}\right] \tag{1.21}$$

$$\beta = \frac{(Offset\ Delay)}{l}\left[2\pi f\sqrt{1-\left(\frac{f_c}{f}\right)^2}\right] \tag{1.22}$$

and

$$Offset\ Loss = \frac{\sqrt{\pi\mu_0 f_c \rho}}{h}\left(\frac{c}{\sqrt{\epsilon_r}}\right), \tag{1.23}$$

$$Offset\ Delay = \frac{l\sqrt{\epsilon_r}}{c}, \tag{1.24}$$

$$w_e = w - \frac{(4-\pi)r^2}{h} \tag{1.25}$$

where
l is the length of the rectangular waveguide section in metres (m),

w, h and r are cross-sectional dimensions of the rectangular waveguide in metres (m),
w is the cross-sectional width in metres (m),
h is the cross-sectional height in metres (m),
r is the edge radius in metres (m),
w_e is the effective guide width in metres (m),
f_c is the cutoff frequency of the waveguide in hertz (Hz) which can be computed using Eq. 1.10,
ρ is the electrical resistivity of the conductor in ohm·metre (Ω·m),
$\mu_0 = 4\pi 10^{-7}$ H/m is the permeability of free space in henry per metre,
$\epsilon_0 = 8.85418782 \times 10^{-12}$ F/m is the permittivity of free space in farad per metre,
ϵ_r is the relative permittivity and
c = 299792458 m/s is the speed of light in vacuum in metres per seconds.

Reciprocal Network

A two port standard that follows the reciprocity condition is known as a reciprocal network. The reciprocity condition is $S_{21} = S_{12}$, which means that the determinant of associated transmission matrix of a reciprocal network must be equal to 1. The reciprocal network can be used as an unknown thru during a calibration procedure.

Some examples of coaxial and waveguide calibration standards are shown in Figs. 1.4 and 1.5 respectively.

Figure 1.4 shows the coaxial 3.5 mm VNA calibration standards [5]. The short, open and load are one port standards while the two port adapter can be used as a thru. These standards are generally used for frequencies up to 26.5 GHz.

The waveguide WR10 calibration standards shown in Fig. 1.5 are one port short and load and two port null shim and offset ($\lambda/4$) shim standards [6]. The frequency of

Fig. 1.4 Calibration kit: Maury microwave 8050CK - coaxial 3.5 mm

Fig. 1.5 Waveguide calibration kit: Agilent model W11644A - WR10

operation for these standards ranges from 75 to 110 GHz. In waveguide environment the open standard does not exist due to the radiation effects at the open end of the waveguide. The combination of short and offset ($\lambda/4$) shim can be used as a realization for an open standard.

1.3.3 Error Box Model

A calibration process characterizes most of the VNA systematic errors. Therefore, before performing the error correction via VNA calibration, it is important to model the systematic errors. This model is known as error box model. It is actually a linear system model in which each parameter is frequency dependent and time invariant. The error box model for a 2-port VNA with four receivers is often referred to as 7-term error model. The VNAs with three receivers require 10-term error model [1]. Here, we will focus only on 7-term error model for the 2-port VNAs.

The error box model of a 2-port VNA is shown in Fig. 1.6. It consists of two error boxes, represented by S-parameter matrices S_x and S_y, between the DUT reference planes and the ideal measurement ports.

The following S-parameter equations can be written for the two error boxes [1]:

$$\begin{bmatrix} V_{x1}^- \\ V_{x2}^- \end{bmatrix} = \underbrace{\begin{bmatrix} e_{11} & e_{10} \\ e_{01} & e_{00} \end{bmatrix}}_{S_x} \begin{bmatrix} V_{x1}^+ \\ V_{x2}^+ \end{bmatrix}, \tag{1.26}$$

and

$$\begin{bmatrix} V_{y1}^- \\ V_{y2}^- \end{bmatrix} = \underbrace{\begin{bmatrix} e_{22} & e_{23} \\ e_{32} & e_{33} \end{bmatrix}}_{S_y} \begin{bmatrix} V_{y1}^+ \\ V_{y2}^+ \end{bmatrix}, \tag{1.27}$$

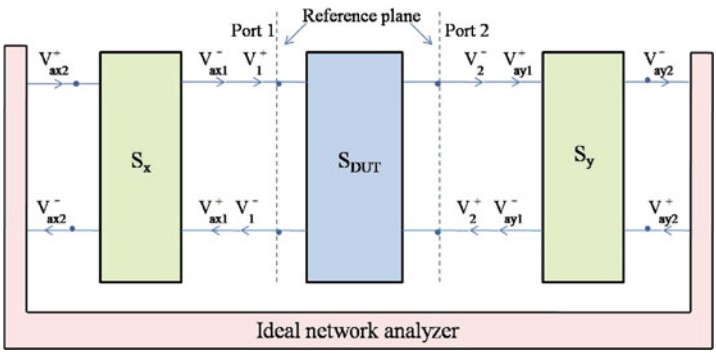

Fig. 1.6 Error box model for a 2-port VNA

where V^- represent the reflected voltage waves and V^+ are the incident voltage waves. The error terms are represented by e. From Eqs. 1.26 and 1.27, it can be observed that there are total eight error terms. Moreover, the error terms e_{01}, e_{10}, e_{23} and e_{32} can never be equal to zero [1]. So, if we assign one of these four error terms to a non-zero value even then the wave quantity ratios remain unaffected. Lets say e_{32} equal to 1, then it implies that only seven independent error terms in the error model to be determined. The error model shown in Fig. 1.6 can be used for forward and reverse measurements.

The systematic errors can be represented by the error terms as follows:

- e_{22} and e_{11} interpreted as load match in forward and reverse measurements respectively
- $e_{10}e_{32}$ and $e_{01}e_{23}$ interpreted as transmission tracking in forward and reverse measurements respectively
- e_{00} and e_{33} interpreted as directivity in forward and reverse measurements respectively
- e_{11} and e_{22} interpreted as source match in forward and reverse measurements respectively
- $e_{10}e_{01}$ and $e_{23}e_{32}$ interpreted as reflection tracking in forward and reverse measurements respectively

A calibration procedure requires one and two port standards to be measured. Lets start with one port standard measurements. If we measure one port standard, with reflection coefficient Γ_s, at port 1, then the measured value can be written as [1]:

$$\frac{{V_{x2}}^-}{{V_{x2}}^+} = e_{00} + \frac{e_{01}e_{10}\Gamma_s}{1 - e_{11}\Gamma_s} \tag{1.28}$$

Similarly, the measurements of one-port standard at port 2 can be formulated as follows:

$$\frac{{V_{y2}}^-}{{V_{y2}}^+} = e_{33} + \frac{e_{23}e_{32}\Gamma_s}{1 - e_{22}\Gamma_s} \tag{1.29}$$

From Eqs. 1.28 and 1.29, it can be seen that one port standard measurements provide to independent equations for the seven unknown error terms. Now, the remaining equations can be obtained from the measurements of the two port standards.

In case of two port standard measurements, the matrices S_x and S_y should be transformed to the corresponding transmission matrices T_x and T_y. Lets assume the two port standard is characterized by the transmission matrix T_s, then the reverse measurements of the two port standard can be modeled as follows [1]:

$$\begin{bmatrix} {V_{x2}}^- \\ {V_{x2}}^+ \end{bmatrix} = \underbrace{T_x T_s T_y}_{T_{Mr}} \begin{bmatrix} {V_{y2}}^+ \\ {V_{y2}}^- \end{bmatrix} \tag{1.30}$$

Similarly, the forward measurements can be formulated as follows:

$$\begin{bmatrix} V_{y2}{}^{-} \\ V_{y2}{}^{+} \end{bmatrix} = T_{Mf} \begin{bmatrix} V_{x2}{}^{+} \\ V_{x2}{}^{-} \end{bmatrix}, \tag{1.31}$$

where T_{Mf} can be obtained from T_{Mr} by matrix transformation.

From Eqs. 1.30 and 1.31, it can be observed that a two port standard measurements provide four equations. If all the standards are fully known, then the calibration will provide eight equations for seven unknown terms. It means that the calibration procedure is overdetermined and we can also use the partially unknown standard for calibration purposes [1].

In next section, the different calibration techniques are discussed that are typically used for the evaluation of unknown error terms.

1.3.4 Calibration Techniques

A calibration technique uses a particular combination of calibration standards to characterize the systematic errors and removes them mathematically during the measurements [7]. Several different calibration techniques are available to calibrate the 2-port VNA [8–29]. Some of the well known calibration techniques for 2-port VNA are as follows:

- Short-Open-Load-Thru (SOLT)
- Thru-Short-Delay (TSD)
- Thru-Reflect-Line (TRL)
- Line-Reflect-Match (LRM)
- Short-Open-Load-Reciprocal (SOLR)
- Enhanced Short-Open-Load-Thru (ESOLT)
- Quick Short-Open-Load-Thru (QSOLT)

SOLT

The SOLT calibration technique [9–13] is a traditional 2-port calibration technique. It requires three one port standards at both test ports and a thru (direct connection). The one port standards used during this calibration are short, open and load standards. The thru connection during calibration identifies only the transmission error coefficients. This calibration technique has redundant standard. The reference impedance of the entire system is set by one of the load standards. Its accuracy highly depends on good standard definition and can be enhanced by improving the calibration standard models [14, 15] or using the standards which are initially characterized using a reference calibration [16].

TSD/TRL

The TSD/TRL calibration techniques are widely used at metrological level. The TSD calibration technique [17, 18] uses a line, one port short standard of known reflection and and a thru (direct connection of two test ports). The one port short

standard is measured at both test ports. On the other hand, TRL [19] uses a line, one port reflect standard of unknown reflection and a thru. The line and the thru must have the same geometry i.e., both must have the same reference impedance. The reference impedance of the system is set by the characteristic impedance of the line. During measurements, the reference plane is placed in the middle of the thru. The length difference between the line and the thru should avoid $\lambda/2$ and its multiples otherwise calibration technique will provide singularity. The TSD/TRL calibration techniques provide accurate transmission and reflection measurements since it is possible to manufacture the line standard with highly precise characteristic impedance.

TSD and TRL calibration techniques are used in coaxial and waveguide environment. However, they can be used for on-wafer measurements where probes can be moved during the calibration. These calibration techniques have bandwidth limitation. For broadband TSD/TRL, more number of lines of different lengths are used. The calibration technique which uses multiple line measurements to broaden the bandwidth of the traditional TRL is known as *Multiline thru-reflect-line (MTRL)* [20–22].

LRM

This calibration technique requires a line, one port reflect standard of unknown reflection and a match standard [23]. The reflect and match standard are measured at both test ports. The reference impedance of the system is set by the load impedance. LRM is a broadband calibration technique because the line standard used during the calibration need not to be of a specific length. However, it is difficult to construct highly precise match standard.

This calibration technique is widely used for on-wafer measurements because it does not require to move the probes during the calibration. It can be as accurate as TRL if the proper match standard is used.

SOLR

The SOLR calibration technique [26] uses three fully known one port standards at both ports and one fully unknown 2-port reciprocal network. The one port standards include short, open and load/match standard. The reciprocal network identifies the transmission error coefficients. The reference impedance of the entire system is set by one of the load standards. It provide accurate reflection measurements but less accurate transmission measurements. The accuracy of the SOLR calibration technique highly depends on the goodness of the one port standards definitions.

This calibration does not require the thru connection. It is useful to perform calibration when two test ports have the same gender.

ESOLT

This calibration technique uses one port short, open and load standards at both test ports and a thru (direct connection). The least square mathematical formulation is used in this calibration technique. Like SOLT, the accuracy of the ESOLT calibration is strongly depends on good standards definitions. The reference impedance of the entire system is set by one of the load standards.

QSOLT

The QSOLT calibration technique [27, 28] requires the measurements of one port short, open and load standards at one VNA port only and a thru (direct connection) between the two test ports. It has no redundant standard. This calibration technique is faster because it require less standards connections during the calibration. The reference impedance is set by the load standard. QSOLT provides accurate transmission measurements but less accurate reflection measurements of the port where standards are not connected during the calibration process.

1.4 Measurement Uncertainty

The residual uncertainty associated with the VNA measurements is important to analyze the results obtained. It is also important to evaluate the sources of error contribution on the final uncertainty and the weight of each component.

1.4.1 Uncertainty Components Classification

Generally, the uncertainty components can be categorized into two classes according to the method used to evaluate them:

Type A

Type A uncertainty evaluation is based on the statistical analysis of a sample of observations. For example, calculating the mean of a series of measurements and then computing the standard deviation of the mean in order to obtain the standard uncertainty.

Type B

Type B uncertainty is evaluated using non statistical methods. It is usually based on scientific judgement of the relevant data or information available. The relevant information can be the data provided by a calibration report, manufacturer's specifications or results of measurements previously performed.

In the VNA measurements, both type A and B uncertainty classification are involved.

1.4.2 Representation of S-Parameter Uncertainty

The S-parameter measurements from the VNA are complex quantities. A complex number is composed of two parts: real and imaginary. A complex number Z, with real part denoted as x and imaginary part denoted as y, can be written as:

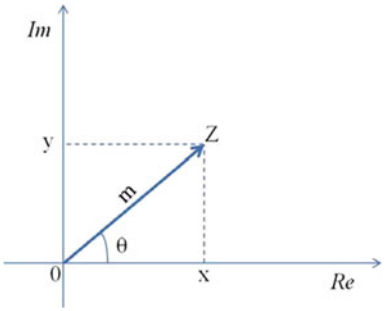

Fig. 1.7 Complex number representation

$$Z = x + iy \tag{1.32}$$

where i is the complex unity. This complex number can be represented in a real/imaginary plane as shown in Fig. 1.7.

The complex number Z can also be represented in magnitude m and phase θ. The non-linear equations that can be used to convert Z from real/imaginary to magnitude/phase form are as follows [30]:

$$m = |Z| = \sqrt{x^2 + y^2} \tag{1.33}$$

and

$$\theta = \angle Z = \begin{cases} arctan(y/x) & \text{if } x > 0 \\ arctan(y/x) + \pi & \text{if } x < 0,\ y \geq 0 \\ arctan(y/x) - \pi & \text{if } x < 0,\ y < 0 \\ \pi/2 & \text{if } x = 0,\ y > 0 \\ -\pi/2 & \text{if } x = 0,\ y < 0 \\ undefined & \text{if } x = 0,\ y = 0 \end{cases} \tag{1.34}$$

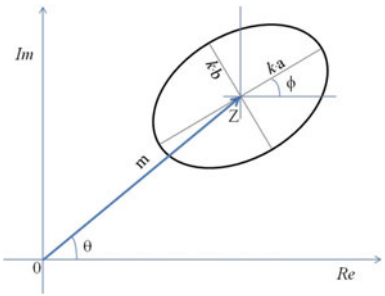

Fig. 1.8 Complex number representation along with uncertainty ellipse. k represents the coverage factor

The uncertainty of a complex number can be represented graphically in the form of an *ellipse* because the residual errors affect both the real and imaginary components. The uncertainty ellipse of the complex number Z is shown in Fig. 1.8. The uncertainty ellipse basically defines a boundary in which "true" value is likely available.

The ellipse axes length and the rotation angle ϕ depend on the variance matrix of complex number Z. It should also be noted that there also exists correlation between the real and imaginary components of the complex number. Therefore, along with the variance of real part V_r and the imaginary part V_i, the covariance between real and imaginary part V_{ri} and V_{ir} also contribute to the final uncertainty assessment [30–35]. By definition, the two covariances V_{ri} and V_{ir} are always equal. The uncertainty variance matrix of a complex number Z can be written in matrix form as follows:

$$V_z = \begin{bmatrix} V_r & V_{ri} \\ V_{ri} & V_i \end{bmatrix} \tag{1.35}$$

The uncertainty ellipse axes length can be computed by evaluating the eigenvalues of the matrix shown in Eq. 1.35. If the eigenvalues of the matrix shown in Eq. 1.35 are λ_1 and λ_2, they can be written mathematically as follows:

$$\lambda_1 = \frac{V_r + V_i + \sqrt{(V_r - V_i)^2 + 4V_{ri}^2}}{2} \tag{1.36}$$

and

$$\lambda_2 = \frac{V_r + V_i - \sqrt{(V_r - V_i)^2 + 4V_{ri}^2}}{2} \tag{1.37}$$

The semi-major and semi-minor axes of the ellipse will be $a = 1/\sqrt{\lambda_2}$ and $b = 1/\sqrt{\lambda_1}$ respectively. The rotation angle ϕ can be written in terms of variances and covariances as follows [30]:

$$\phi = \frac{1}{2} \arctan\left(-\frac{2V_{ri}}{V_r - V_i}\right) \tag{1.38}$$

As mentioned earlier that the uncertainty ellipse defines a boundary in which the "true" value lies with some probability. In order to increase the probability that the "true" value lies within the bounded region defined by ellipse, the major and minor axis lengths can be enlarged by a coefficient called *coverage factor*. In Fig. 1.8, the coverage factor is denoted by k. The coverage factor basically expands the uncertainty and increases the level of confidence to get the "true" value. For scalar quantities with normal probability distribution, the coverage factor commonly used are the following:

- k = 1 for 68 % level of confidence;
- k = 2 for 95 % level of confidence;
- k = 3 for 99 % level of confidence.

However, for complex quantities, the coverage factor k = 2 will no longer gives an expanded uncertainty with 95 % level of confidence. Therefore, for complex quantities, the coverage factor k is given as the square root of the 95 % point of χ^2-distribution with two degrees of freedom, one for each component of the complex quantity. Generally, for an n-port network, the coverage factor for 95 % level of confidence is given as follows:

$$k = \sqrt{\chi^2_{p,0.95}}, \tag{1.39}$$

where $p = 2n^2$ and $\chi^2_{p,0.95}$ is the 95 % point of χ^2-distribution having p degrees of freedom [31].

A similar concept applies to S-parameters as well. Each S-parameter is a complex quantity and has its own associated uncertainty. There exists a correlation between real and imaginary parts of a S-parameter. The correlation also exists between different S-parameters. So, both the variance of a S-parameter and the covariance between two S-parameters contribute to the uncertainty assessment. The variance matrix $V_{S_{mn}}$ of a S-parameter S_{mn} can be written as follows:

$$V_{S_{mn}} = \begin{bmatrix} V_{ReS_{mn}} & V_{ReS_{mn}ImS_{mn}} \\ V_{ImS_{mn}ReS_{mn}} & V_{ImS_{mn}} \end{bmatrix} \tag{1.40}$$

where $V_{ReS_{mn}}$ and $V_{ImS_{mn}}$ are the variances of the real and imaginary parts of S_{mn} respectively. While $V_{ReS_{mn}ImS_{mn}}$ is the covariance between the real and imaginary parts of S_{mn}. By definition $V_{ReS_{mn}ImS_{mn}}$ and $V_{ImS_{mn}ReS_{mn}}$ are equal.

Similarly, the covariance matrix $V_{S_{mn}S_{ij}}$ between the two S-parameters S_{mn} and S_{ij} can be expressed as follows:

$$V_{S_{mn},S_{ij}} = \begin{bmatrix} V_{RRS_{mn}S_{ij}} & V_{RIS_{mn}S_{ij}} \\ V_{IRS_{mn}S_{ij}} & V_{IIS_{mn}S_{ij}} \end{bmatrix} \tag{1.41}$$

where $V_{RRS_{mn}S_{ij}}$ is the covariance between the real part of S_{mn} and the real part of S_{ij} and $V_{IIS_{mn}S_{ij}}$ is the covariance between the imaginary part of S_{mn} and the imaginary part of S_{ij}. The matrix elements $V_{RIS_{mn}S_{ij}}$ and $V_{IRS_{mn}S_{ij}}$ are the real-imaginary and imaginary-real covariances of S_{mn} and S_{ij} respectively. In general, the matrix elements $V_{RIS_{mn}S_{ij}}$ and $V_{IRS_{mn}S_{ij}}$ are not equal. Both variance and covariance matrices are of size 2×2.

The complete variance/covariance matrix of a network can be written based on variance and covariances matrices described above. For a 2-port network, the complete variance/covariance matrix $V_{s,2p}$ will becomes:

$$V_{s,2p} = \begin{bmatrix} V_{S_{11},S_{11}} & V_{S_{11},S_{12}} & V_{S_{11},S_{21}} & V_{S_{11},S_{22}} \\ V_{S_{12},S_{11}} & V_{S_{12},S_{12}} & V_{S_{12},S_{21}} & V_{S_{12},S_{22}} \\ V_{S_{21},S_{11}} & V_{S_{21},S_{12}} & V_{S_{21},S_{21}} & V_{S_{21},S_{22}} \\ V_{S_{22},S_{11}} & V_{S_{22},S_{12}} & V_{S_{22},S_{21}} & V_{S_{22},S_{22}} \end{bmatrix} \tag{1.42}$$

where each element of the $V_{s,2p}$ matrix is a 2×2 real matrix. Similarly, an n-port network contains n^2 S-parameters, which implies that the complete variance/covariance matrix of a n-port network consists of n^4 variance and covariance matrices, each of size 2×2.

The diagonal elements of complete variance/covariance matrix can be used to compute the uncertainty of magnitude and phase quantities of S-parameters by using the *Gaussian Error Propagation* that, according to [36], is defined by the following equations:

$$u(|Z|) = \sqrt{\left(\frac{\partial|Z|}{\partial x}\right)^2 \sigma_x^2 + \left(\frac{\partial|Z|}{\partial y}\right)^2 \sigma_y^2 + 2\left(\frac{\partial|Z|}{\partial x}\right)\left(\frac{\partial|Z|}{\partial y}\right)\sigma_{xy}}, \tag{1.43}$$

and

$$u(\theta_Z) = \sqrt{\left(\frac{\partial\theta}{\partial x}\right)^2 \sigma_x^2 + \left(\frac{\partial\theta}{\partial y}\right)^2 \sigma_y^2 + 2\left(\frac{\partial\theta}{\partial x}\right)\left(\frac{\partial\theta}{\partial y}\right)\sigma_{xy}}, \tag{1.44}$$

where, $|Z| = \sqrt{x^2 + y^2}$ and $\theta_Z = \arctan(y/x)$ are the modulus and the phase of a complex number Z respectively, while $u(|Z|)$ and $u(\theta_Z)$ are the standard uncertainties for magnitude and phase respectively. σ_x^2 and σ_y^2 are the variances of the real and imaginary parts x and y respectively, while σ_{xy} is the covariance between real and imaginary part of the complex number. The expanded uncertainty "U" can be computed from the standard uncertainty "u" as follows:

$$U = ku, \tag{1.45}$$

where, the coverage factor k depends on the desired level of confidence.

The mathematical modelling of the uncertainty associated with the VNA measurements and its analytical treatment will be discussed in Chap. 2. The interaction of different uncertainty sources and their propagation to the final DUT uncertainty will also be presented.

References

1. Hiebel M (2007) Fundamentals of vector network analysis, 2nd edn. Rohde and Schwarz GmbH & Co., Germany ISBN 978-3-939837-06-0
2. Gonzalez G (1999) Microwave transistor amplifier: analysis and design, Chap. 1, Sect. 1.4, 2nd edn. Prentice-Hall, Inc., Englewood Cliffs, N.J, USA
3. Agilent PNA calibrate measurements—measurement errors. http://na.tm.agilent.com/pna/help/WebHelp7_5/S3_Cals/Errors.htm#errsys
4. Agilent, Agilent application note 1287-11, specifying calibration standards and kits for agilent vector network analyzers. http://www.agilent.com
5. 3.5mm Calibration kits, coaxial VNA calibration kits—series 8050CK—datasheet. https://www.maurymw.com/pdf/datasheets/2Z-059.pdf

6. Agilent technologies WR-10 mechanical calibration kit—user manual. http://cp.literature.agilent.com/litweb/pdf/11644-90369.pdf
7. Rumiantsev A, Ridler N (2008) VNA calibration. IEEE Microw Mag 9(3):86–99 June
8. Eul HJ, Schiek B (1991) A generalized theory and new calibration procedures for network analyzer self-calibration. IEEE Trans Microw Theory Tech. 39(4):724–731
9. Kruppa W (1971) An explicit solution for the scattering parameters of a linear two-port measured with an imperfect test set. IEEE Trans Microw Theory Tech MTT–19(1):122–123
10. Rehnmark S (1974) On the calibration process of automatic network analyzer systems. IEEE Trans Microw Theory Tech 22(4):457–458
11. Engen GF (1974) Calibration technique for automated network analyzers with application to adapter evaluation. IEEE Trans Microw Theory Tech MTT–22:1255–1260
12. Franzen NR, Speciale RA (1975) A new procedure for system calibration and error removal in automated sparameter measurements. In: Proceedings of the 5th European microwave conference (Hamburg). pp 69–73
13. Fitzpatrick J (1978) Error models for system measurement. Microw J 21:63–66 May
14. Padmanabhan S, Kirby P, Daniel J, Dunleavy L (2003) Accurate broadband on-wafer SOLT calibrations with complex load and thru models. In Proceedings of the 61st ARFTG microwave measurements conference. Springer, Heidelberg, pp 5–10
15. Blackham D, Wong K (2005) Latest advances in VNA accuracy enhancements. Microw J 48:78–94 July
16. Ridler N, Nazoa N (2006) Using simple calibration load models to improve accuracy of vector network analyser measurements. In: Proceedings of the 67th ARFTG microwave measurements conference. Springer, Heidelberg, pp 104–110
17. Engen GF, Hoer CA (1978) The application of thru-short-delay to the calibration of the dual six-port. In: IEEE-MTT-S international microwave symposium digest. pp 184–185
18. Engen GF, Hoer CA (1979) Thru-load-delay: an improved technique for calibrating the dual six-port. In: IEEE-MTT-S international microwave symposium digest. p 53 (1979)
19. Engen GF, Hoer CA (1979) Thru-reflect-line: an improved technique for calibrating the dual six port automatic network analyzer. IEEE Trans Microw Theory Tech MTT–27:987–993
20. Marks RB (1991) A multiline method of network analyzer calibration. IEEE Trans Microw Theory Tech 39(7):1205–1215
21. Williams DF, Wang JCM, Arz U (2003) An optimal vector-network-analyzer calibration algorithm. IEEE Trans Microw Theory Tech 51(12):2391–2401
22. Williams DF, Marks RB, Davidson A (1991) Comparison of on-wafer calibrations. In: Proceedings of the 38th ARFTG microwave measurements conference. Fall, pp 68–81
23. Eul HJ, Schiek B (1988) Thru-match-reflect: one result of a rigorous theory for de-embedding and network analyzer calibration. In: Proceedings of the 18th European microwave conference. Stockholm, Sweden, pp 909–914
24. Soares RA, Gouzien P, Legaud P, Follot G (1989) A unified mathematical approach to two-port calibration techniques and some applications. IEEE Trans Microw Theory Tech 37:1660–1674
25. Silvonen KI (1991) Calibration of test fixtures using at least two standards. IEEE Trans Microw Theory Tech 39:624–630 Apr
26. Ferrero A, Pisani U (1992) Two-port network analyzer calibration using an unknown thru. IEEE Microw Guided Wave Lett 2(12):505–507 Dec
27. Ferrero A, Pisani U (1991) QSOLT: A new fast calibration algorithm for two port S parameter measurements. In: 38th ARFTG conference digest. San Diego, CA, pp 15–24
28. Eul HJ, Schiek B (1991) Reducing the number of calibration standards for network analyzer calibration. IEEE Trans Instrum Meas 40(4):732–735
29. Shoaib N (2012) A novel inconsistency condition for 2-port vector network analyzer calibration. Microw Opt Technol Lett 54(10):2372–2375 Oct
30. MMS application note AN-202.2, Part 2: understanding complex numbers uncertainty. http://www.hfemicro.com/pdf/MMS4_AN-202-2.pdf
31. Ridler NM, Salter MJ (2002) An approach to the treatment of uncertainty in complex S-parameter measurements. Metrologia 39(3):295–302

32. Hall BD (2003) Calculating measurement uncertainty for complex-valued quantities. Meas Sci Technol 14(3):368–375
33. Hall BD (2010) Notes on complex measurement uncertainty—Part 1, Industrial Research Ltd., New Zealand. Technical report 2483
34. Hall BD (2012) Notes on complex measurement uncertainty—Part 2, Industrial Research Ltd., New Zealand. Technical report 2557
35. Hall BD (2007) Some considerations related to the evaluation of measurement uncertainty for complex-valued quantities in radio frequency measurements. Metrologia 44(6):L62–L67
36. Taylor JR (1982) An introduction to error analysis, the study of uncertainties in physical measurements, 2nd edn. University Science Books, Sausalito, CA, pp 209–914

Chapter 2
Waveguide Measurement Uncertainty

Abstract This chapter will deal with the analytical treatment of the VNA measurement uncertainty evaluation. In particular, the measurement uncertainty evaluation for the waveguide standards will be presented. The uncertainty propagation flowchart highlighting the interaction of different measurement uncertainty sources will be discussed. The dimensional characterization of the waveguide standards will also be described.

2.1 Introduction

Waveguide is a structure that guides electromagnetic or sound waves. The most common waveguide has a hollow metallic structure. The waveguides found numerous applications in communication systems. The development of reliable communication systems is highly based on the precise and reliable network analysis. Therefore, the measurement uncertainty assessment is critical for the traceable measurements. In this chapter, the waveguide measurement uncertainty evaluation is discussed.

As an example, the scattering parameter (S-parameter) measurements using a VNA for two different waveguide sets of type WR15 and WR10 are discussed [1–3]. The frequency ranges from 50 to 110 GHz. The uncertainty analysis is carried out for the waveguide standards. The mechanical characterization of the waveguide standards is also the part of the discussion. The waveguide measurement results are also compared with the theoretical electromagnetic computations based on mechanical characterization of the WR15 and WR10 shims, that are included in the standards, to assess the compatibility between the data.

2.2 Mathematical Model and Measurement Uncertainty Evaluation

This section will present the VNA calibration model and the measurement uncertainty evaluation using an analytical approach. A two-state hardware VNA calibration

N. Shoaib, *Vector Network Analyzer (VNA) Measurements and Uncertainty Assessment*, PoliTO Springer Series, DOI 10.1007/978-3-319-44772-8_2

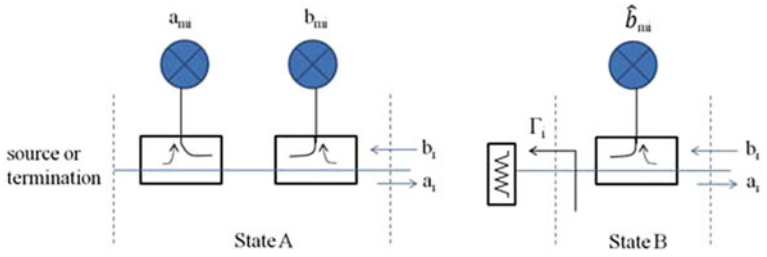

Fig. 2.1 Two-state hardware model [4]

model is described [4]. The S-parameter uncertainty evaluation using a fully analytical approach described in [5] is also highlighted.

The two-state hardware VNA model is the extension of the complete reflectometer multi-port VNA non-leaky model [6] to the non-complete reflectometer architecture. In the two-state model, each VNA port has two different states as shown in Fig. 2.1. *State A* represents the traditional complete reflectometer in which incident and the reflected waves are measurable. *State B* is the partial reflectometer in which only reflected wave is measurable.
State A can be represented mathematically as follows [7]:

$$\begin{aligned} a_i &= l_i b_{mi} - h_i a_{mi} \\ b_i &= k_i b_{mi} - m_i a_{mi} \end{aligned} \tag{2.1}$$

While the mathematical formulations for the *State B* are as follows [4]:

$$\begin{aligned} a_i &= g_i \hat{b}_{mi} \\ b_i &= f_i \hat{b}_{mi} \end{aligned} \tag{2.2}$$

The port i reflectometer termination in *State B* i.e. Γ_i, is always the same for each port j source excitation with $i \neq j$ [4]. The error coefficients l_i, m_i, h_i, k_i, f_i and g_i must be computed firstly for each port and then the corrected S-parameter data is obtained using a de-embedding procedure. The measurements are linked to the corrected waves by the following de-embedding equation [4]:

$$\underbrace{(\mathbf{K}\mathbf{B}_m - \mathbf{M}\mathbf{A}_m + \mathbf{F}\hat{\mathbf{B}}_m)}_{\mathbf{B}} = \mathbf{S}\underbrace{(\mathbf{L}\mathbf{B}_m - \mathbf{H}\mathbf{A}_m + \mathbf{G}\hat{\mathbf{B}}_m)}_{\mathbf{A}} \tag{2.3}$$

where, **K**, **M**, **F**, **L**, **H** and **G** are diagonal matrices containing the error coefficients. **H**, **K** and **F** contain the transmission error coefficients, while **M**, **L** and **G** contain the reflection error coefficients. The matrices $\mathbf{A}_m$, $\mathbf{B}_m$ and $\hat{\mathbf{B}}_m$ contain the measurements. The Eq. 2.3 is also used for calibration.

The measurement uncertainty is very useful for measurement process since it provides information about the main error sources. The error sources can be

analyzed and reduced to get accurate measurements. Using the VNA calibration model, the measurement uncertainty of a device under test (DUT) can be formulated. The differentiation of (2.3) gives the following uncertainty propagation equation [8]:

$$\delta \mathbf{S} = (\delta \boldsymbol{\beta}_e + \delta \boldsymbol{\beta}_m)(\mathbf{A})^{-1} \tag{2.4}$$

where:

$$\delta \boldsymbol{\beta}_e = [(\delta \mathbf{K} - \mathbf{S}\delta \mathbf{L})\mathbf{B}_m - (\delta \mathbf{M} - \mathbf{S}\delta \mathbf{H})\mathbf{A}_m + (\delta \mathbf{F} - \mathbf{S}\delta \mathbf{G})\hat{\mathbf{B}}_m] \tag{2.5}$$

and

$$\delta \boldsymbol{\beta}_m = [(\mathbf{K} - \mathbf{SL})\delta \mathbf{B}_m - (\mathbf{M} - \mathbf{SH})\delta \mathbf{A}_m + (\mathbf{F} - \mathbf{SG})\delta \hat{\mathbf{B}}_m]. \tag{2.6}$$

The terms $\delta \boldsymbol{\beta}_e$ and $\delta \boldsymbol{\beta}_m$ provide the contributions due to uncertainties in the error coefficients and measurement noise during the DUT measurement, respectively. $\delta \boldsymbol{\beta}_e$ and $\delta \boldsymbol{\beta}_m$ represent different uncertainty sources, therefore, both terms are completely independent. The uncertainty sources considered are the following:

- Standard definition
- Measurement noise
- Connector/cable repeatability

The definition of a calibration standard can affects the measurement accuracy i.e. standard fabrication can impact the final accuracy of the calibration standard. However, this uncertainty contribution can be simulated using the Monte Carlo methods for final measurement uncertainty evaluation.

The measurement noise can be classified into low-level and high-level noise sources (see Chap. 1, Sect. 1.3.1). It can be characterized by performing the repeated raw measurements using a matched load a short at the test port [5]. However, due to high dynamic ranges of the VNAs, this uncertainty contribution usually has the least significant impact on the final measurement uncertainty.

The connector/cable repeatability analysis is helpful to understand the variability of the repeated VNA measurements. Particularly, at millimeter frequencies, a slight misalignment of the waveguide flange will give rise to reflections at the interface which can cause systematic and random errors in the electrical measurements. A detailed connection repeatability investigation of the VNA at millimetre frequencies is also presented in Chap. 4.

The different uncertainty sources are propagated with respect to the specific DUT measurements to compute the final uncertainty. The uncertainty propagation flowchart is shown in Fig. 2.2. It is evident from Fig. 2.2 that the uncertainty propagation interacts in a complex way up to the final DUT measurement. The standard definition uncertainty affects the error coefficients estimation and indirectly the DUT measurement. The measurement noise uncertainty contribution occurs during the calibration and the DUT measurement. The connector/cable repeatability affects the standard

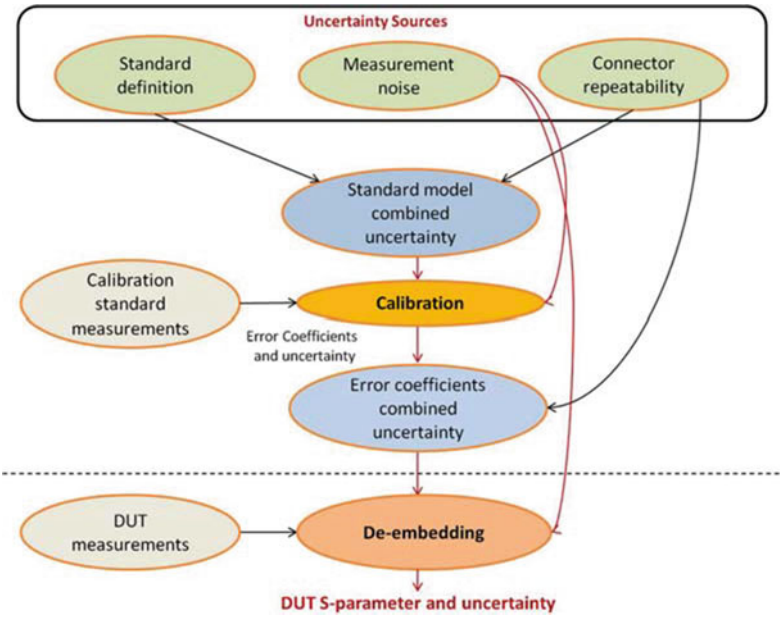

Fig. 2.2 Uncertainty propagation flowchart [5]

model combined uncertainty and the de-embedding process. The detailed theoretical and mathematical analysis of S-parameter uncertainty assessment is described in [5]. This mathematical approach for uncertainty evaluation is compliant with the *Guide to the expression of uncertainty in measurements* (GUM) [9].

In addition to the uncertainty propagation, the choice of the VNA calibration technique is also very critical since it affects the final measurement accuracy. This fact is highlighted in Chap. 3 in which a comparison between the two different VNA calibration techniques is discussed in terms of S-parameter measurements and related uncertainty at millimeter frequencies.

The variances and co-variances of the measured scattering parameters (S-parameters) also affect the final measurement uncertainty. For a 2-port network, the variance between S-parameters can be written, e.g. for S_{11}, as:

$$\overline{\delta S_{11}\delta S_{11}^{*}} = \sum_{r=1,2}\sum_{t=1,2}[(A^{-1})_{r1}\overline{\delta\beta_{1r}\delta\beta_{1t}^{*}}(A^{-1})_{t1}^{*}] \tag{2.7}$$

and

$$\overline{\delta\beta_{1r}\delta\beta_{1t}^{*}} = \overline{\delta\beta_{e,1r}\delta\beta_{e,1t}^{*}} + \overline{\delta\beta_{m,1r}\delta\beta_{m,1t}^{*}} \tag{2.8}$$

where the bar indicates the statistical average and $\delta\beta_{e,1r}$, $\delta\beta_{e,1t}$, $\delta\beta_{m,1r}$ and $\delta\beta_{m,1t}$ are the elements of $\delta\beta_e$ and $\delta\beta_m$. $\delta\beta^*_{e,1t}$ and $\delta\beta^*_{m,1t}$ are the complex conjugate of $\delta\beta_{e,1t}$ and $\delta\beta_{m,1t}$ respectively.

The variance/covariance matrix $V_{s,2p}$ of the measured 2-port S-parameter will become:

$$V_{s,2p} = \begin{bmatrix} \overline{\delta S_{11}\delta S^*_{11}} & \overline{\delta S_{11}\delta S^*_{12}} & \overline{\delta S_{11}\delta S^*_{21}} & \overline{\delta S_{11}\delta S^*_{22}} \\ \overline{\delta S_{12}\delta S^*_{11}} & \overline{\delta S_{12}\delta S^*_{12}} & \overline{\delta S_{12}\delta S^*_{21}} & \overline{\delta S_{12}\delta S^*_{22}} \\ \overline{\delta S_{21}\delta S^*_{11}} & \overline{\delta S_{21}\delta S^*_{12}} & \overline{\delta S_{21}\delta S^*_{21}} & \overline{\delta S_{21}\delta S^*_{22}} \\ \overline{\delta S_{22}\delta S^*_{11}} & \overline{\delta S_{22}\delta S^*_{12}} & \overline{\delta S_{22}\delta S^*_{21}} & \overline{\delta S_{22}\delta S^*_{22}} \end{bmatrix} \tag{2.9}$$

Each element of the $V_{s,2p}$ matrix is a 2×2 real matrix. For example, $\overline{\delta S_{11}\delta S^*_{11}}$ can be written in matrix form as:

$$\overline{\delta S_{11}\delta S^*_{11}} = \begin{bmatrix} \sigma^2_{ReS_{11}} & \sigma_{ReS_{11}ImS_{11}} \\ \sigma_{ImS_{11}ReS_{11}} & \sigma^2_{ImS_{11}} \end{bmatrix}, \tag{2.10}$$

where, $\sigma^2_{ReS_{11}}$ and $\sigma^2_{ImS_{11}}$ are the variances of the real and imaginary parts of S_{11} respectively, while $\sigma_{ReS_{11}ImS_{11}}$ is the covariance between real and imaginary part of S_{11}. The diagonal elements of the $V_{s,2p}$ matrix can be used to compute the uncertainty of S-parameters using the *Law of Propagation of Uncertainty* [9, 10] using the Eqs. 1.43 and 1.44 described in Chap. 1, Sect. 1.4.2.

The VNA calibration model and the S-parameter uncertainty evaluation described above are implemented in a software package namely, *Microwave Measurement Software version 4.0* (MMS4). This software is based on a fully analytical approach for uncertainty assessment described in [5]. It considers the correlation between real and imaginary part of complex-valued S-parameter and provides full covariance matrix of S-parameters. MMS4 is developed by High Frequency Engineering (HFE) [11] to perform advanced multi-port microwave measurements and uncertainty evaluation. In the following sections, an example related to the S-parameter measurements and uncertainty assessment using a VNA for two different waveguide sets of type WR15 and WR10 is presented.

2.3 Measurands and Measurement Setup

The standards consisted of two calibration kits. The first one is a WR15 waveguide calibration kit of frequency range 50–75 GHz while the second one is a WR10 waveguide calibration kit of frequency range 75–110 GHz. Each calibration kit contained a short, a load, a $\lambda/4$ shim and a 5 cm line that are used as devices under test (DUTs). The calibration kits are *Agilent Technologies* mod. V11644A for WR15 and mod. W11644A for WR10 waveguide. The TRL calibration technique [12] is used for the VNA calibration. The measurands are the one-port reflection coefficient for

Fig. 2.3 Measurement setup

loads and shorts (S_{11}) and the complete S-parameter measurement set for shims and lines (S_{11}, S_{22}, S_{21}, S_{12}).

The measurement setup employed is a two-port VNA (*Agilent Technologies* mod. E8364C) covering the frequency range of 10 MHz to 50 GHz. Two millimeter wave extenders (*OML* V15VNA2-T/R and V10VNA2-T/R for WR15 and WR10 waveguide respectively) are used to extend the frequency range up to 110 GHz. In order to have precise port alignment, the millimeter wave extenders are placed onto a custom-made translation stage having 6 degrees of freedom. The measurements are performed in a shielded room that has stable temperature (23.0 °C ± 0.3 °C) and relative humidity (45 % ± 5 %).

The VNA is operated at nominal power levels of +8 dBm and +5 dBm for WR-15 and WR-10 waveguide respectively. The measurements are repeated five times at each frequency by reconnecting the DUTs each time in order to take into consideration the connection repeatability. A pictorial view of the measurement setup is shown in Fig. 2.3. The measurements are performed at National Institute of Meteorological Research - INRIM, Italy.

2.4 Dimensional Measurements

The dimensional measurements are carried out at INRIM in order to compute the theoretical S-parameters along with associated uncertainties. The WR15 and WR10

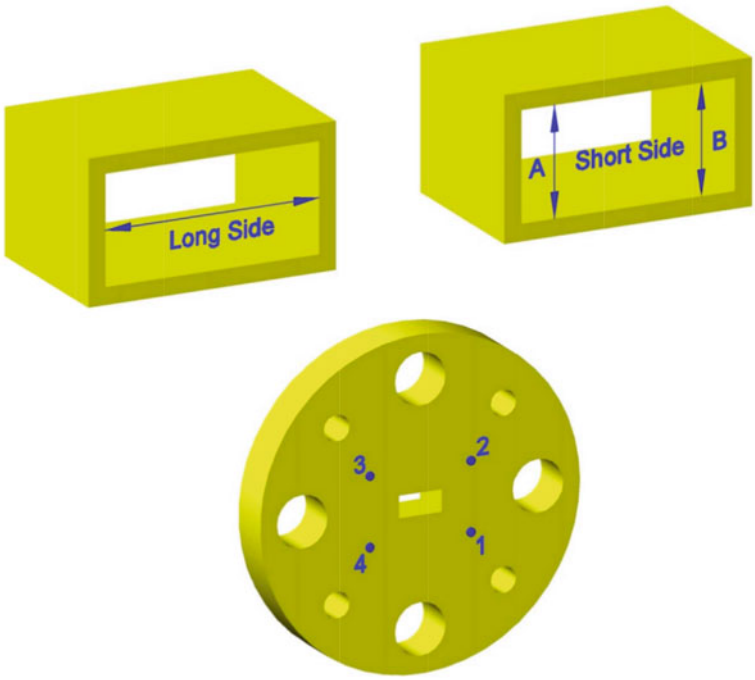

Fig. 2.4 Shim dimensional measurement layout

shims, used as DUTs, are mechanically characterized [13] in order to provide an additional verification of the electromagnetic measurements.

The mechanically measured shims are the null shim and the offset ($\lambda/4$) shim. The mechanically measured parameters include the cross-sectional height, width and length of the rectangular waveguide located at the centre of the shim. The shorter side of the rectangular waveguide is measured in two symmetrical sections "A" and "B" with respect to the central section, while the longer side is measured in the central section as shown in Fig. 2.4. The thickness measurements are carried out at four points which are distributed centrally around the side of the rectangular hole as depicted in the same figure. A similar mechanical measurement procedure is adopted for both null and offset ($\lambda/4$) shims.

The first step for mechanical characterization of shim is to determine the measuring position. This is determined by mounting the shim on an interferometric 1D comparator with a contact probe. The side under examination is aligned with the comparator measuring axis, using the longer side of the waveguide rectangular hole as a reference. For thickness measurement, the shim is vertically placed on a mounting with the measurement sides perpendicular to the measurement axis of the 1D comparator. The Z movements of the contact probe on one side of the shim verified the vertical alignment. The probe contacts and the interferometric readings at four symmetrical positions at the corners of the central rectangular hole are acquired on

both faces of the shim. Due to the small dimensions of the inner wall, the measuring probe could not measure its roughness. The corrections in interferometric readings are carried out for the refractive index of air, which is calculated from the environmental parameters acquired during the test execution, and for the temperature of the DUT. The wavelength in vacuum of the laser interferometer is calibrated by comparison with the national standard of length. The diameter of the contact sphere and the constant of the proportional probe are determined using a dimensional reference standard (INRIM certified) mounted on the same 1D comparator.

The uncertainty of the dimensional measurements is 1.5 μm. This uncertainty is basically the standard deviation of the repeated dimensional measurements. The uncertainty of the measuring instruments is 0.1 μm, which is much smaller than the uncertainty of the dimensional measurements. The expected theoretical S-parameter along with uncertainties are computed using the dimensional measurements and their associated uncertainties. Both reflection and transmission S-parameters are computed.

The reflection S-parameters are computed using the Eq. (2.3) mentioned in [14] for rectangular waveguide standards, while the transmission parameters are computed according to the *Waveguide Calibration Coefficient Mathematical Model* [15], described by the Eqs. 1.21 and 1.22 discussed in Chap. 1, Sect. 1.3.2. The resistivity of 22.14 nΩ/m is used as provided by the manufacturer. The uncertainties for the computed S-parameter are evaluated according to the GUM [9].

2.5 Measurement Results

The measurements and the uncertainty assessments are performed for short, load, shim and line standards, included in both the WR15 and WR10 calibration kits. Some results are presented here both in graphical and numerical form. Figures 2.5, 2.6, 2.7 and 2.8 present the reflection coefficient measurements along with associated uncertainties for WR15 and WR10 short standards. Figures 2.9, 2.10, 2.11 and 2.12 show the transmission coefficients for WR15 and WR10 line standards. The expanded uncertainties of transmission coefficient phase measurements for WR15 and WR10 line standards are magnified by a factor of 50 for better presentation as shown in Figs. 2.10 and 2.12. Data reported in Table 2.1 shows the comparison between computed and measured transmission coefficients of WR15 and WR10 shims. The coverage factor $k = 2$ is used, to give a level of confidence of 95 %, to compute the expanded uncertainty U from combined standard uncertainty.

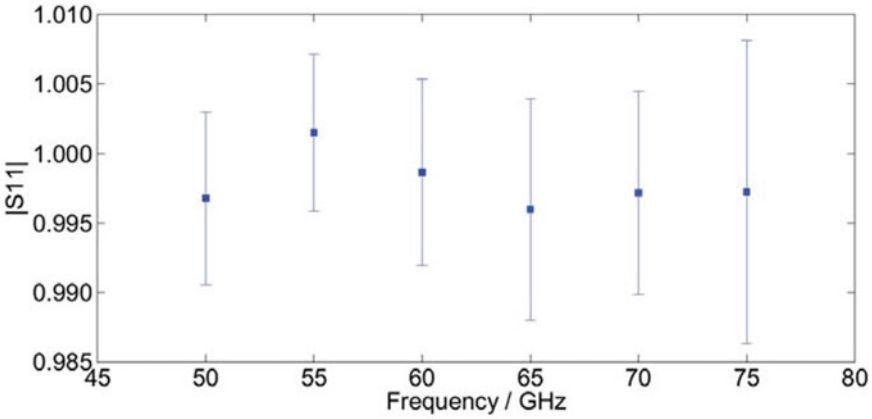

Fig. 2.5 $|S_{11}|$ for Short WR15 standard

2.6 Uncertainty Budget

In this section, an example of uncertainty budget is presented in order to demonstrate the contribution of each individual uncertainty component to the final combined standard uncertainty.

Table 2.2 shows an uncertainty budget highlighting the different uncertainty contributions for WR15 and WR10 short standard measurements at specific frequency point. The measurement uncertainty assessment follow the analytical approach described in [5]. The uncertainty components considered are connector/cable repeatability, measurement noise and standard definitions. The different standard uncertainty contributions are combined as root sum of the squares to form the *combined standard uncertainty*.

2.7 Discussion

An analytical evaluation of the agreement between the computed and the measured transmission coefficients can be performed through the compatibility index (I) that, according to [16], is defined for scalar quantities (such as S-parameter magnitude and phase) by the following equation:

$$I = \left(K_U^c - K_U^m\right)\left[U^2(K_U^c) + U^2(K_U^m)\right]^{-\frac{1}{2}}, \tag{2.11}$$

(c=computed, m=measured), where K_U is the measurand value and $U(K_U)$ is the associated expanded uncertainty of the measurand. The discrepancies between

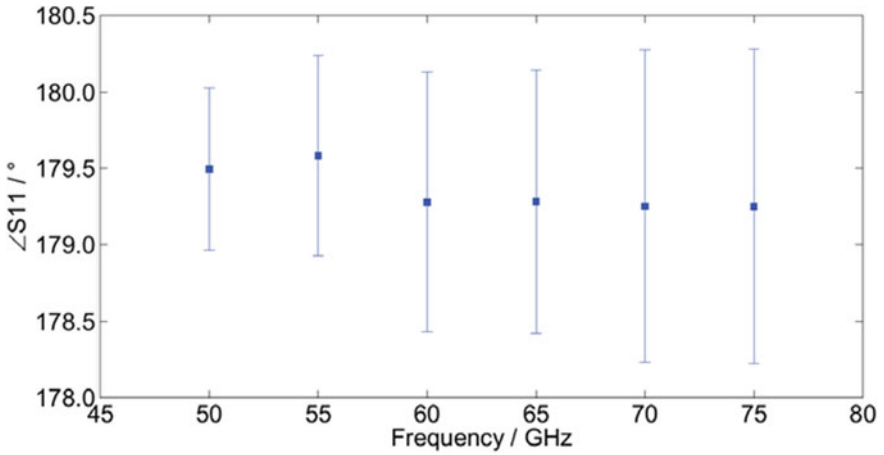

Fig. 2.6 $\angle S_{11}/°$ for Short WR15 standard

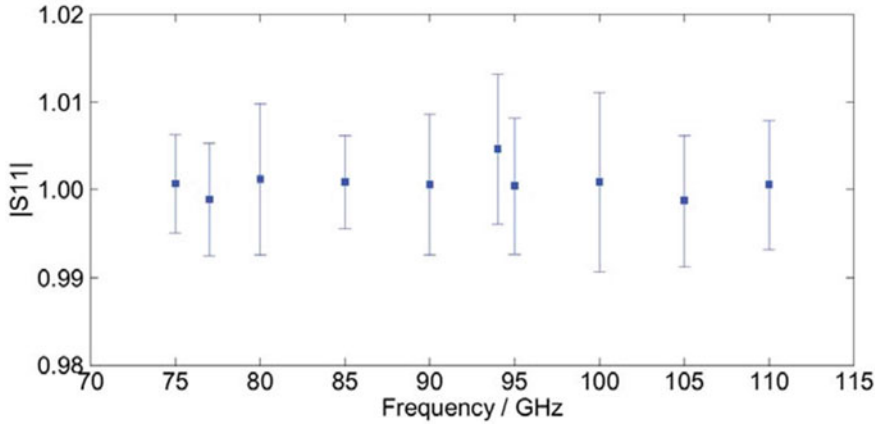

Fig. 2.7 $|S_{11}|$ for Short WR10 standard

data are acceptable as statistic fluctuations if the compatibility index (2.11) is, in modulus, ≤ 1.

The compatibility index I between the computed and the measured transmission coefficient data, as shown in Table 2.1, satisfies the compatibility condition for all the compared S-parameter data and show a high degree of compatibility. The same compatibility indexes are evaluated for all the results, providing always satisfying agreements.

The characteristic parameters of every standard of the TRL calibration kit are taken into account in the calculation and their uncertainty propagated, through the mathematical model adopted, to the final results. Moreover, the uncertainty evaluation approach allows to fully take into account the correlation between real and

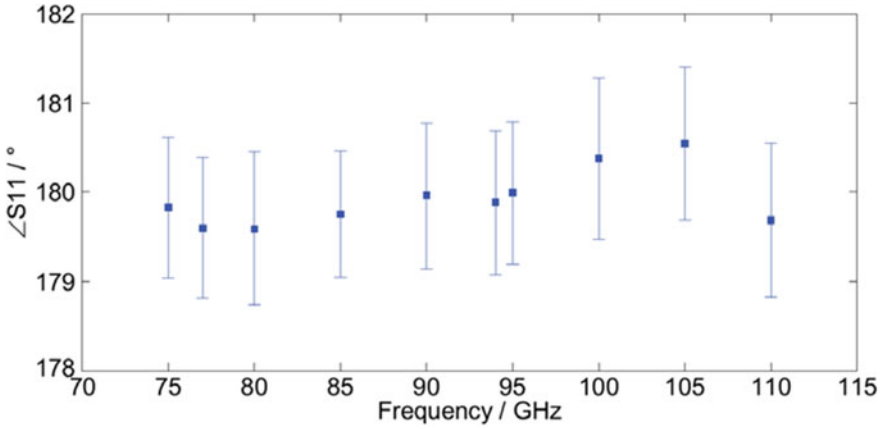

Fig. 2.8 $\angle S_{11}/°$ for Short WR10 standard

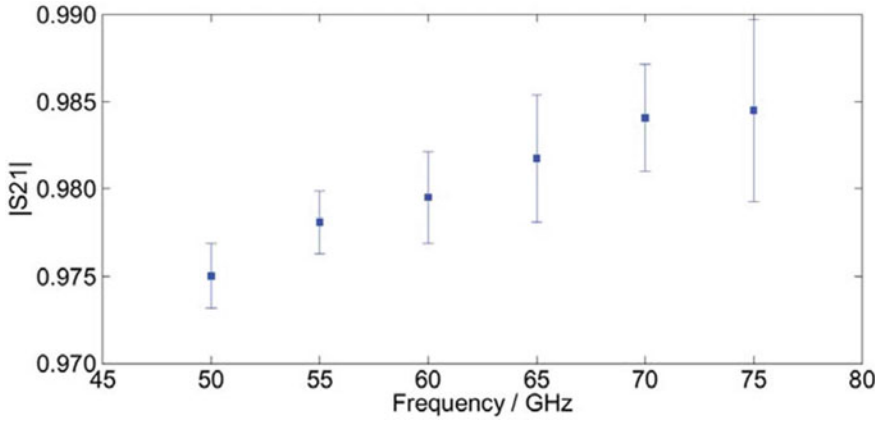

Fig. 2.9 $|S_{21}|$ for Line WR15 standard

imaginary parts of the S-parameters. The reflection S-parameter results are shown greater than 1 at some frequencies due to the fact that, by assumption, the uncertainty bars are considered symmetrical.

2.8 Conclusion

In this chapter the waveguide measurements and uncertainty analysis are discussed. The mathematical formulation for measurement uncertainty is presented. The propagation of different VNA uncertainty sources is also discussed. The uncertainty evaluation approach is used to compute the measurement uncertainty for the one and

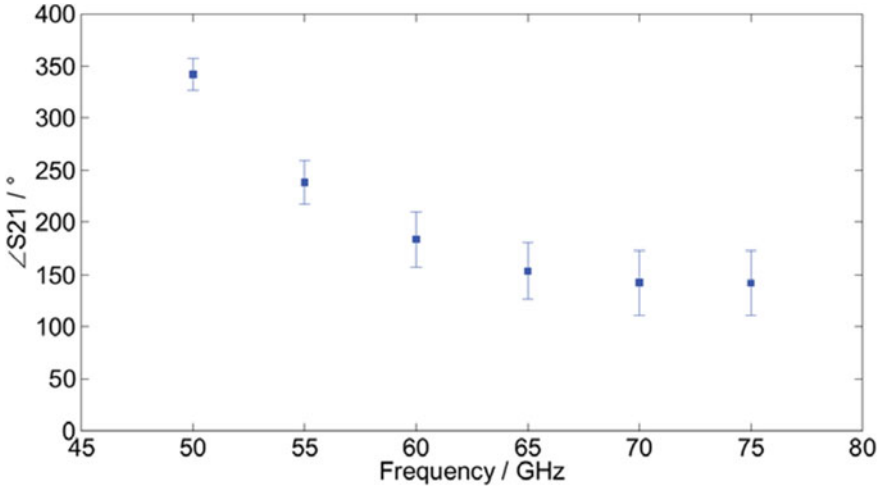

Fig. 2.10 $\angle S_{21}/°$ for Line WR15 standard. The expanded uncertainties are magnified by a factor of 50 for better reading

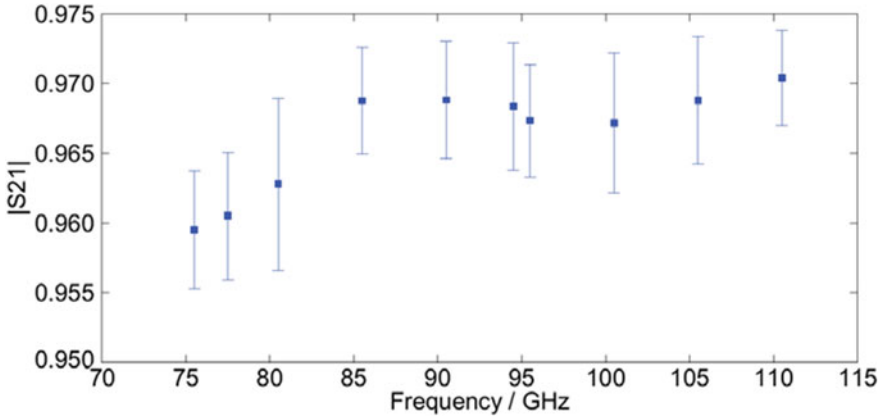

Fig. 2.11 $|S_{21}|$ for Line WR10 standard

two port travelling standards at millimeter frequencies (50–110 GHz). All the measurement data turned out to be compatible to the theoretical computed data within stated uncertainties.

The VNA model and the analytical treatment of uncertainty presented in this chapter can be used for other VNA waveguide test setups. This uncertainty approach also includes the correlation between real and imaginary part of complex-valued S-parameters thus providing a more realistic estimate of the final measurement uncertainty.

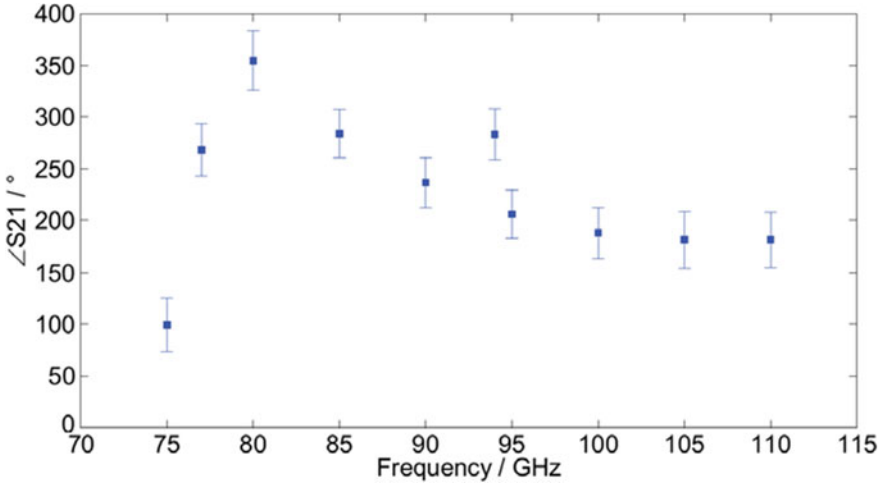

Fig. 2.12 $\angle S_{21}/°$ for Line WR10 standard. The expanded uncertainties are magnified by a factor of 50 for better reading

Table 2.1 Shim ($|S_{21}|$) WR15 and WR10 Measurements. I represents the compatibility index between the computed and the measured transmission coefficient data

	Computed data		Measured data		
f(GHz)	$\|S_{21}\|$	$U(\|S_{21}\|)$	$\|S_{21}\|$	$U(\|S_{21}\|)$	$\|I\|$
50	0.9996	0.0012	0.9987	0.0019	0.3910
55	0.9996	0.0010	1.0005	0.0018	0.4155
60	0.9997	0.0009	0.9991	0.0027	0.2003
65	0.9997	0.0009	0.9988	0.0037	0.2345
70	0.9997	0.0008	1.0004	0.0031	0.2166
75	0.9997	0.0008	0.9999	0.0053	0.0350
75	0.9995	0.0015	1.0005	0.0044	0.2183
77	0.9995	0.0014	1.0011	0.0048	0.3179
80	0.9995	0.0013	1.0005	0.0064	0.1470
85	0.9996	0.0012	1.0024	0.0039	0.6921
90	0.9996	0.0011	1.0038	0.0044	0.9245
94	0.9996	0.0011	0.9979	0.0047	0.3541
95	0.9996	0.0011	1.0039	0.0042	0.9874
100	0.9996	0.0011	1.0008	0.0052	0.2214
105	0.9996	0.0010	0.9995	0.0047	0.0278
110	0.9996	0.0010	1.0009	0.0035	0.3454

Table 2.2 Short ($|S11|$) WR15 and WR10 uncertainty budget

Uncertainty source	Probability distribution	Standard uncertainty	
		WR15 @ 55 GHz	WR10 @ 95 GHz
Conn. repeatability	Normal	0.00272	0.00176
Noise	Normal	0.00080	0.00344
Standard definition	Normal	0.00009	0.00007
Expanded uncertainty ($k = 2$)		0.00567	0.00773

References

1. Yueyan S, Oberto L, Meng YS, Neo H, Brunetti L,Sellone M (2012) Scattering parameter measurement comparison between NMC and INRIM on vector network analyzer using WR15 and WR10 connectors. In: Conference on Precision Electromagnetic Measurements (CPEM) (2012), pp 96–97
2. Sellone M, Oberto L, Shan Y, Meng YS, Brunetti L, Shoaib N (2013) Comparison of S-parameter measurements at millimeter wavelengths between INRIM and NMC. IEEE Trans Instrum Meas 63(7):1810–1817
3. Shoaib N, Sellone M, Oberto L, Brunetti L, Shan Y, Meng YS (2014) Phase comparison between NMC and INRIM on scattering parameter measurements with WR15 and WR10 connections. In: Conference on precision electromagnetic measurements (CPEM 2014), Rio de Janeiro, Brazil, pp 168–169, 24–29 Aug 2014
4. Ferrero A, Teppati V, Garelli M, Neri A (2008) A novel calibration algorithm for a special class of multiport vector network analyzer. IEEE Trans Microw Theory Tech 56:693–699
5. Garelli M, Ferrero A (2012) A unified theory for S-parameter uncertainty evaluation. IEEE Trans Microw Theory Tech 60(12):3844–3855
6. Ferrero A, Sanpietro F (1995) A simplified algorithm for leaky network analyzer calibration. IEEE Micro Guide Wave Lett 5(4):119–121
7. Ferrero A, Pisani U, Kerwin K (1992) A new implementation of a multiport automatic network analyzer. IEEE Trans Microw Theory Tech. 40(11):2078–2085
8. Ferrero A, Garelli M, Grossman B, Choon S, Teppati V (2011) Uncertainty in multiport S-parameters measurements. In: 77th IEEE microwave measurement conference (ARFTG), pp 1–4
9. BIPM, IEC, IFCC, ILAC, ISO, IUPAC, IUPAP and OIML (2008) JCGM 100:2008, evaluation of measurement data—guide to the expression of uncertainty in measurement. International Organization for Standardization (ISO). http://www.bipm.org/en/publications/guides/gum.html
10. Taylor JR (1982) An introduction to error analysis, the study of uncertainties in physical measurements., 2nd edn. University Science Books, Sausalito
11. HFE high frequency engineering, Sagl Zona Industriale San Vittore (GR), Switzerland, http://www.HFEmicro.ch
12. Engen GF, Hoer CA (1979) Thru-reflect-line: an improved technique for calibrating the dual six port automatic network analyzer. IEEE Trans Microw Theory Tech 27:987–993
13. Bellotti R (2012) Rapporto di prova n. 12–0051-01. Technical report, Istituto Nazionale di Ricerca metrologica - INRIM, Torino
14. Dudley RA, Ridler NM (2003) Traceability via the internet for microwave measurements using vector network analyzers. IEEE Trans Instrum Meas 52(1):130–134
15. Agilent, Agilent application note 1287-11. Specifying calibration standards and kits for agilent vector network analyzers, http://www.agilent.com
16. European co-operation for accreditation, EA-02/03 guide. Interlaboratory comparison. http://www.european-accreditation.org

Chapter 3
VNA Calibration Comparison

Abstract A VNA calibration procedure characterizes and reduces the systematic errors of the instrumentation from the raw measurement data. The measurement accuracy mainly depends on the quality of the VNA calibration. Therefore, the choice of the calibration procedure is very critical. The goal of this chapter is present a comparison of the state of the art 2-port VNA calibration techniques at millimetre frequencies. This comparison will be useful to analyze the efficiency of two different VNA calibration techniques.

3.1 Introduction

A calibration technique is a critical procedure to obtain the accurate measurements using the VNA [1]. During past decades, the research work on VNA calibrations has been carried out in depth and their advantages and disadvantages have been published. There are several calibration algorithms are available to calibrate the 2-port VNAs [2–23]. In this chapter, the state of the art 2-port calibration techniques Thru-Reflect-Line (TRL) [13] and Quick Short-Open-Load-Thru (QSOLT) [21, 22] will be discussed and compared. For comparison purposes, the measurement results obtained from TRL and QSOLT calibration techniques in WR10 waveguide will be presented as an example [24, 25].

The aim of this comparison is to analyze the efficiency of two different VNA calibration techniques in terms of S-parameter measurements and related uncertainty at millimeter frequencies using a fully analytical approach [26] already discussed in Chap. 2, Sect. 2.2. This comparison used the mechanical characterization of the WR10 waveguide as standard definitions and propagated them to evaluate the final uncertainties. The applicability of QSOLT as a calibration technique for waveguide measurements traceable to the *International System of units* (SI) has also been verified. Several works are presented in the past concerning the S-parameters measurement and uncertainty evaluation using VNA calibration techniques. Some of them either dealt with a specific calibration technique at microwave frequencies [27, 28] or used different calibration techniques at same frequencies [29–31]. The guidelines on the evaluation of vector network analyzers, *EURAMET* guide [32], are also

N. Shoaib, *Vector Network Analyzer (VNA) Measurements and Uncertainty Assessment*, PoliTO Springer Series, DOI 10.1007/978-3-319-44772-8_3

based on assumption of zero reflection for precision transmission line. However, this assumption is demonstrated invalid due to the systematic reflection coefficients of the connectors, as described in [33]. The work presented in [34] is based on a heavy numerical approach and limited to coaxial standards up to microwave frequencies. The uncertainty analysis using a fully analytical approach has already been presented in [26] but limited to the coaxial standards up to microwave frequencies. This chapter will present the VNA calibration comparison using a fully analytical approach [26] for WR10 waveguide standards.

3.2 Calibration Techniques

The TRL and QSOLT calibration techniques are already discussed in Chap. 1-Sect. 1.3.4. The TRL calibration technique is generally considered as one of the most accurate calibration technique. It requires one port reflect standard of unknown reflection, a thru and a line of different length whose characteristic impedance sets the reference impedance of the measurement system. The knowledge of line length is not necessarily required to perform the calibration. However, in the case of precise computation of propagation constant, this knowledge is necessary [13]. This calibration technique is typically used at metrological level.

The QSOLT uses one port short, open and load standards at one port only and a thru connection. The reference impedance is set by the load standard. This calibration is faster to perform because it requires less standard connections. The level of accuracy for transmission measurements is good. However, the reflection measurements are less accurate for the port where the calibration standards are not connected while performing the calibration [21, 22]. The choice of calibration technique is critical and it affects the measurement accuracy. The calibration standards required for performing TRL and QSOLT calibration techniques are also shown in Table 3.1.

Table 3.1 Standards required to perform TRL and QSOLT calibration techniques

Calibration technique	Standards required
TRL	Thru
	Unknown reflect
	Line
QSOLT	Short
	Open
	Load
	Thru

3.3 Measurement Uncertainty Evaluation

The S-parameter uncertainty is evaluated using a fully analytical approach described in [26]. The detailed mathematical model and uncertainty assessment are already discussed in Chap. 2-Sect. 2.2. The uncertainty sources considered are standard definitions, measurement noise and connector/cable repeatability. The uncertainty sources are propagated with respect to the specific device under test (DUT) measurements to compute the final uncertainty. The mathematical approach followed for uncertainty evaluation is compliant with the *Guide to the expression of uncertainty in measurements* (GUM) [35]. For S-parameter measurements and uncertainty evaluation, a software namely, *Microwave Measurement Software version 4.0* (MMS4) is used. This software is based on a fully analytical approach for uncertainty assessment described in [26] and developed by High Frequency Engineering (HFE) [36].

3.4 Measurands and Measurement Setup

The reference standards used for VNA calibration consisted of a WR10 commercial VNA calibration kit, of *Oleson Microwave Labs* (OML) mod. V10-AL-33, covering the frequency range 75–110 GHz. For TRL calibration technique, a direct connection between the two test ports is used as a thru, the short standard connected at both port 1 and 2 as reflect standard and the offset ($\lambda/4$) shim as line standard. For QSOLT calibration, short is used as short standard, offset ($\lambda/4$) shim + short (offset-short) as an open standard, null shim + short (offset-short) as load standard and a direct connection between the two test ports as thru. The short, open and load standards are connected at port 1 only. The offset ($\lambda/4$) shim + short (offset-short) is used as a realization for an open standard because an open standard doesn't exist in waveguide calibration kits due to radiation effects at the open end of the waveguide. Also, the null shim + short (offset-short) is used as load standard because the null shim + short (offset-short) can easily be mechanically characterized as compared to a match standard. A summary of calibration standards used for this comparison exercise is shown in Table 3.2. The precision load and line standards belonging to the WR10 waveguide calibration kit of *Hewlett Packard* (HP) mod. W11644A are used as DUTs. The measurands are the reflection coefficients of the precision load and line (S_{11}, S_{22}) and the transmission coefficients of the same precision line standard (S_{21}, S_{12}).

The measurement setup used is a two-port VNA (*Agilent Technologies* mod. E8364C) covering the frequency range of 10 MHz to 50 GHz. The WR10 millimeter wave extenders (*OML* V10VNA2-T/R) are used to extend the frequency range to 75–110 GHz. The measurements are performed in a shielded room that has stable temperature (23.0 °C ± 0.3 °C) and relative humidity (45 % ± 5 %). The VNA is operated at nominal power levels of +5 dBm. The pictorial view of the measurement setup is already shown in Fig. 2.3 of Sect. 2.3 in Chap. 2.

Table 3.2 Standards used for calibration comparison

Calibration technique	Standards used
TRL	Thru (direct connection)
	Short
	Offset ($\lambda/4$) Shim
QSOLT	Short
	Offset ($\lambda/4$) Shim + Short
	Null Shim + Short
	Thru (direct connection)

3.5 Dimensional Characterization

The WR10 shims, belonging to the calibration kit used to calibrate the VNA, are mechanically characterized [37] in order to obtain a realistic uncertainty of the calibration standards. The mechanically measured shims are the null shim and the offset ($\lambda/4$) shim. The mechanically measured parameters include the cross-sectional height, width and length of the rectangular waveguide located at the centre of the shim. The complete dimensional measurement procedure is already discussed in Chap. 2-Sect. 2.4.

The expected theoretical S-parameter values along with uncertainties are computed using the dimensional measurements and their associated uncertainties. The reflection parameters are computed using the mathematical equations reported in [1, Sect. 3.3.2] for rectangular waveguide standards. The transmission parameters are computed according to the *Waveguide Calibration Coefficient Mathematical Model* [38] using the Eqs. 1.21 and 1.22 described in Chap. 1-Sect. 1.3.2. In addition, the *Monte Carlo* simulations with 10,000 iterations are used to compute the S-parameters real/imaginary variances and co-variances for one port and two port standards. The *Monte Carlo* approach is chosen because it is computationally less extensive as well as more flexible than any analytical derivation as recommended in [26]. The computed S-parameters real/imaginary variances and co-variances for one port and two port standards using the *Monte Carlo* simulations have then been inserted into the database of the MMS4 software. The software then computed the standard definition uncertainties for one and two port devices using the real/imaginary variances and covariances data according to the GUM [35].

3.6 Measurement Results

The 2-port TRL and QSOLT calibrations are implemented using the WR10 standards. For TRL calibration, a thru (direct connection between the two test ports), a short standard at port 1 and 2 and an offset ($\lambda/4$) shim are measured. The measurements of these calibration standards are saved. In order to perform the QSOLT

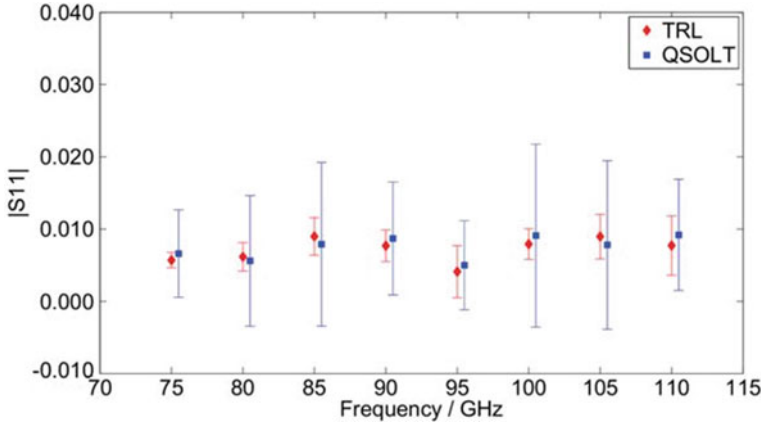

Fig. 3.1 $|S_{11}|$ for WR-10 load using TRL and QSOLT calibrations. The frequency axis is slightly shifted for better presentation

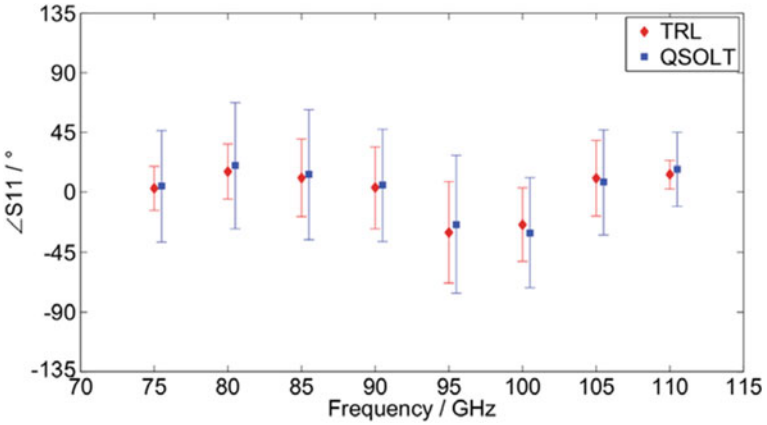

Fig. 3.2 $\angle S_{11}/°$ for WR-10 load using TRL and QSOLT calibrations. The frequency axis is slightly shifted for better presentation

calibration, the open (offset $(\lambda/4)$ shim + short) and load (null shim + short) are measured only and the previously measurements saved during the TRL calibration of short and thru standards are used to avoid any additional repeatability error. The TRL and QSOLT calibrations are then used to correct the raw data for the WR10 load and line standards used as DUTs. Figures 3.1, 3.2, 3.3 and 3.4 present the reflection coefficient measurements along with associated uncertainties for WR10 load standard. The transmission coefficient measurements along with associated uncertainties

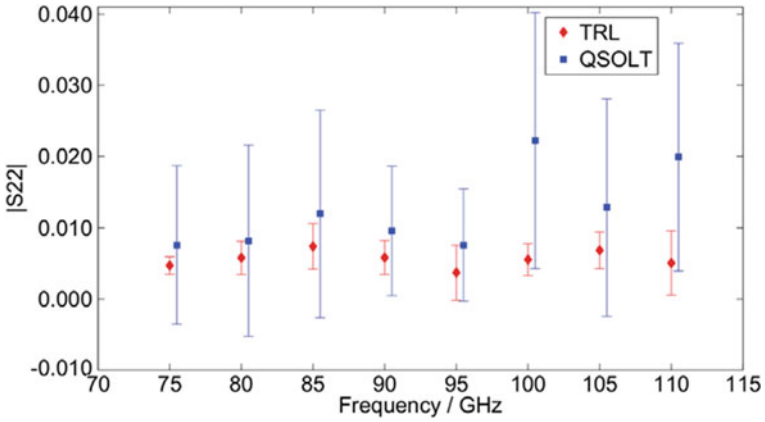

Fig. 3.3 $|S_{22}|$ for WR-10 load using TRL and QSOLT calibrations. The frequency axis is slightly shifted for better presentation

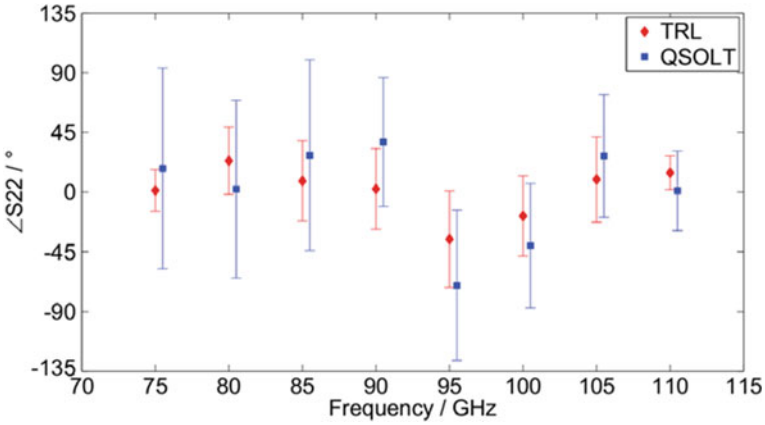

Fig. 3.4 $\angle S_{22}/°$ for WR-10 load using TRL and QSOLT calibrations. The frequency axis is slightly shifted for better presentation

are presented in Figs. 3.5 and 3.6. The expanded uncertainties of transmission coefficient phase measurements for the line standard are magnified by a factor of 50 for better presentation as shown in Fig. 3.6. The load measurement results are presented at port 1 and 2 in order to highlight the fact that the QSOLT provides less accurate reflection measurements of the port where the standards are not connected during the calibration. The coverage factor $k = 2$ is used for 95 % confidence interval to compute the expanded uncertainty U from combined standard uncertainty.

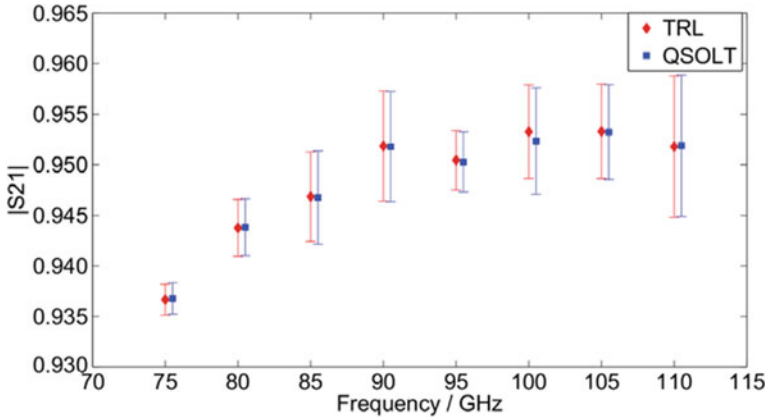

Fig. 3.5 $|S_{21}|$ for WR-10 line using TRL and QSOLT calibrations. The frequency axis is slightly shifted for better presentation

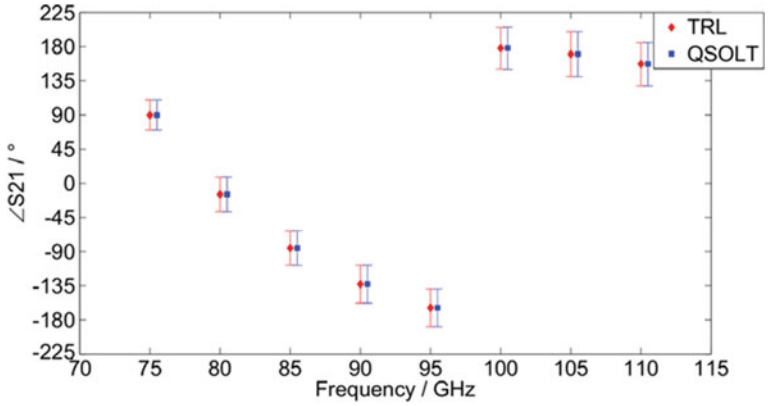

Fig. 3.6 $\angle S_{21}/^\circ$ for WR-10 line using TRL and QSOLT calibrations. The expanded uncertainties are magnified by a factor of 50 for better reading. The frequency axis is slightly shifted for better presentation

3.7 Uncertainty Budget

An example of the uncertainty budget at 90 GHz is shown in Table 3.3, for the reflection coefficient of load WR10 standard at port 2, in order to demonstrate the contribution of each individual uncertainty component to the final combined standard uncertainty. The uncertainty components considered are connector/cable repeatability, measurement noise and standard definitions. The uncertainty contributions are assumed to have normal probability density function (pdf). The different standard uncertainty contributions are combined as root sum of the squares to form the *combined standard uncertainty*.

Table 3.3 Load WR10 uncertainty budget at 90 GHz

Uncertainty source	Standard uncertainty			
	Load WR10 ($\lvert S_{22}\rvert$)		Load WR10 ($\angle S_{22}/°$)	
	TRL	QSOLT	TRL	QSOLT
Conn. repeatability	0.00119	0.00395	15.2073	15.7380
Noise	0.00003	0.00047	0.1687	2.8105
Standard definition	0.00002	0.00221	0.7265	18.3867
Expanded uncertainty ($k = 2$)	0.00238	0.00910	30.4512	48.7300

3.8 Discussion

There exists a good agreement between the results obtained using the TRL and QSOLT calibration techniques, as evident from Figs. 3.1, 3.2, 3.3, 3.4, 3.5 and 3.6. Particularly, the transmission coefficients and the associated uncertainties obtained using the TRL and QSOLT calibrations agreed to each other very well as depicted in Figs. 3.5 and 3.6. Some significant differences exist between the TRL and QSOLT calibrations for reflection coefficient measurements of load standard at port 2 as shown in Figs. 3.3 and 3.4. This is due to fact that the the QSOLT, by definition, had no reflection standard connected at port 2 during calibration process due to which the noise occurred during measurements at port 2 and provided less accurate results as compared to TRL. Also, it can be observed that the uncertainty obtained using QSOLT calibration is always higher than the TRL for reflection measurements. This can be due to following reasons: QSOLT had no reflection connection at port 2 which has resulted in noise uncertainty contribution to become higher than the one for TRL; QSOLT used greater number of one port standards as compared to TRL and this has caused the higher standard definition uncertainty; the connector repeatability is also higher for QSOLT. The repeatability uncertainty contribution takes into account both repeatability affecting the calibration standards and the DUT measurements as described in [26]. The uncertainty budget example shown in Table 3.3 also highlights these facts.

3.9 Conclusion

In this chapter the WR10 waveguide measurements and uncertainty analysis comparison using two different VNA calibration techniques are described. The calibration comparison involved the comparison of TRL and QSOLT calibration techniques in

terms S-parameter measurements and associated uncertainty of one and two port standards at millimeter frequencies (75–110 GHz). The S-parameter results demonstrated that the TRL calibration technique is preferable as compared to QSOLT, for the reflection measurements of one and two ports DUTs. However, the two techniques provided same level of accuracy for the transmission measurements. Anyways, the QSOLT can be applied to waveguide standards. Being all the calibration standards mechanically measurable, the QSOLT can be a metrological alternative calibration technique to TRL at millimetric bands for tracing S-parameter measurements to the *SI*.

References

1. Hiebel M, (2007) "Fundamentals of Vector Network Analysis", 2nd edn, Rohde & Schwarz GmbH & Co., Germany. ISBN 978-3-939837-06-0
2. Eul HJ, Schiek B (1991) A generalized theory and new calibration procedures for network analyzer self-calibration. IEEE Trans. Microwave Theory Tech. 39(4):724–731
3. Kruppa W, Sodomsky KF (1971) "An explicit solution for the scattering parameters of a linear two-port measured with an imperfect test set", *IEEE Trans. Microwave Theory Tech.*, vol. MTT-19(1): 122–123
4. Rehnmark S (1974) On the calibration process of automatic network analyzer systems. IEEE Trans. Microwave Theory Tech. 22(4):457–458
5. Engen GF (1974) "Calibration technique for automated network analyzers with application to adapter evaluation", IEEE Trans. Microwave Theory Tech. MTT-22:1255–1260
6. Franzen NR, Speciale RA (1975) "A new procedure for System Calibration and error removal in automated Sparameter measurements". In: Proceedings of the 5th European Microwave Conference (Hamburg) pp 69–73
7. Fitzpatrick J (1978) Error models for system measurement. Microwave Journal 21:63–66
8. Padmanabhan S, Kirby P, Daniel J, Dunleavy L (2003) "Accurate broadband on-wafer SOLT calibrations with complex load and thru models", In: Proceedings of the 61st ARFTG Microwave Measurements Conference Berlin,Springer, p. 5–10
9. Blackham D, Wong K (2005) Latest advances in VNA accuracy enhancements. Microwave Journal 48:78–94
10. Ridler N, Nazoa N (2006) "Using simple calibration load models to improve accuracy of vector network analyser measurements", In: Proceedings of the 67th ARFTG Microwave Measurements Conference, Springer, Berlin, pp. 104–110
11. Engen GF, Hoer CA (1978) "The Application of "Thru-Short-Delay" to the Calibration of the Dual Six-Port", IEEE-MTT-S International Microwave Symposium Digest, pp. 184–185
12. Engen GF, Hoer CA (1979) "Thru-Load-Delay: An Improved Technique for Calibrating the Dual Six-Port", IEEE-MTT-S International Microwave Symposium Digest, p 53
13. Engen GF, Hoer CA (1979) "Thru-reflect-line: An improved technique for calibrating the dual six port automatic network analyzer", IEEE Trans. Microwave Theory Tech. MTT-27: 987–993
14. Marks RB (1991) A multiline method of network analyzer calibration. IEEE Trans. Microwave Theory Tech. 39(7):1205–1215
15. Williams DF, Wang JCM, Arz U (2003) An optimal vector-network-analyzer calibration algorithm. IEEE Trans. Microwave Theory Tech. 51(12):2391–2401
16. Williams DF, Marks RB, Davidson A (1991) "Comparison of on-wafer calibrations", In: Proceedings of the 38th ARFTG Microwave Measurements Conference Fall, pp 68–81
17. Eul HJ, Schiek B (1988) "Thru-match-reflect: One result of a rigorous theory for de-embedding and network analyzer calibration", In: Proceedings of the 18th European Microwave Conference Stockholm, Sweden, pp 909–914

18. Soares RA, Gouzien P, Legaud P, Follot G (1989) A unified mathematical approach to two-port calibration techniques and some applications. IEEE Trans. Microwave Theory Tech. 37:1660–1674
19. Silvonen KI (1991) Calibration of test fixtures using at least two standards. IEEE Trans. Microwave Theory Tech. 39:624–630
20. Ferrero A, Pisani U (1992) Two-Port Network Analyzer calibration using an unknown thru. IEEE Microwave and Guided Wave Letters 2(12):505–507
21. Ferrero A, Pisani U (1991) "QSOLT: A new fast calibration algorithm for two port S parameter measurements", In: Proceedings of the 38th ARFTG Conf. Dig., San Diego, CA, pp 15–24
22. Eul HJ, Schiek B (1991) Reducing the number of calibration standards for network analyzer calibration. IEEE Trans. Instrum. Meas. 40(4):732–735
23. Shoaib N (2012) A novel inconsistency condition for 2-port vector network analyzer calibration. Microwave Opt. Technol. Lett. 54(10):2372–2375
24. Shoaib N, Sellone M, Ferrero A, Oberto L, Brunetti L (2013) "Error propagation with different calibration techniques at millimeter frequencies", In: Proceedings of the 82nd ARFTG Microwave Measurement Symposium, Columbus, Ohio, USA, pp 1–3
25. Shoaib N, Sellone M, Oberto L, Brunetti L (2014) "Error propagation with TRL and QSOLT calibration techniques at millimeter frequencies", INRIM technical report, T.R. 14/2014, pp 1–22
26. Garelli M, Ferrero A (2012) "A Unified Theory for S-parameter Uncertainty Evaluation", IEEE Trans. Microwave Theory Tech. 60(12):3844–3855
27. Stumper U (2005) Uncertainty of VNA S-parameter measurement due to nonideal TRL calibration items. IEEE Trans. Instrum. Measure. 54:676–679
28. Williams D, Wang C (2003) "An optimal multiline TRL calibration algorithm", MTT-S International Microwave Symposium Digest, pp 1819–1822
29. Sanpietro F, Ferrero A, Pisani U, Brunetti L (1995) "Accuracy of a multiport vector network analyzer", IEEE Trans. Instrum. Measure. 44(2):304–307
30. Martens J, Judge D, Bigelow J (2004) "Uncertainties associated with many-port (>4) S-parameter measuremets using a four port vector network analyzer", IEEE Trans. Microwave Theory Tech. MTT-52(5):1361–1368
31. Stumper U (2007) Uncertainties of VNA S-parameter measurements applying the TAN self-calibration method. IEEE Trans. Instrum. Measure. 56:597–600
32. European Association of National Metrology Institutes (EURAMET), "EURAMET cg-12 v.2.0, guidelines on the evaluation of vector network analyzers (VNA)", March 2011 [Online]. http://www.euramet.org/index.php?id=calibration-guides
33. Hoffmann J, Leuchtman P, Ruefenacht J, Wong K (2009) "S-parameters of slotted and slotless coaxial connectors", In: Proceedings of the 74th ARFTG Microwave Measurement Symposium, pp 1–5
34. Wollensack M (2012) "VNA Tools II: S-parameter uncertainty calculation", In: Proceedings of the 79th ARFTG Microwave Measurement Conference, p 1–5
35. BIPM, IEC, IFCC, ILAC, ISO, IUPAC, IUPAP and OIML, "JCGM 100:2008, evaluation of measurement data-Guide to the expression of uncertainty in measurement", International Organization for Standardization (ISO), Sep. 2008 [Online]. http://www.bipm.org/en/publications/guides/gum.html
36. "HFE High Frequency Engineering Sagl Zona Industriale San Vittore (GR)", Switzerland [Online]. http://www.HFEmicro.ch
37. Bellotti R (2013) Rapporto di prova n. 13–0323-01. Tech. Rep, Istituto Nazionale di Ricerca metrologica - INRIM, Torino
38. Agilent, "Agilent Application Note 1287-11, Specifying Calibration Standards and Kits for Agilent Vector Network Analyzers", [Online]. http://www.agilent.com

Chapter 4
VNA Connection Repeatability Investigation

Abstract The connection repeatability is one of the uncertainty sources associated with the VNA measurements. Its investigation is helpful to understand the variability of the repeated VNA measurements. In this chapter, the connection repeatability investigation of the VNA at millimetre frequencies will be presented. The mathematical formulations for the connection repeatability will also be described.

4.1 Introduction

The dimensions of the standard waveguide aperture become smaller with an increase in operating frequency. Particularly, at millimeter frequencies, these dimensions aperture become very small i.e. of the order of mm. Therefore, accurate and repeatable dimensional alignment of the waveguide becomes very important in order to have reliable and repeatable scattering parameter (S-parameter) measurements. A slight misalignment of the waveguide will give rise to reflections at the interface. This misalignment will cause systematic and random errors in the electrical measurements. Therefore, this connection repeatability investigation is important to analyze the variability of the repeated measurements and flange alignment mechanisms.

This chapter presents the connection repeatability investigation of the VNA at millimetre frequencies. In particular, the connection repeatability investigation for the WR05 waveguide standards over the frequency range of 140–220 GHz is discussed [1]. Four one-port devices are investigated: (i) a flush short-circuit; (ii) an offset short-circuit; (iii) a near-matched termination; and (iv) a mismatched termination. These devices can be used as the standards for calibrating the VNAs. The experimental standard deviation is computed to observe the variability in the measurement results due to the flange connection repeatability. The repeatability analysis is performed separately for both the real and imaginary parts of the complex-valued measured reflection coefficient. Each DUT is measured 10 times under essentially the same repeatability conditions of measurement ([2]: ISO JCGM 200:2012 Sect. 2.20).

N. Shoaib, *Vector Network Analyzer (VNA) Measurements and Uncertainty Assessment*, PoliTO Springer Series, DOI 10.1007/978-3-319-44772-8_4

4.2 Mathematical Formulation

The connection repeatability can be defined as the standard deviation in the measured S-parameter of a waveguide standard. The experimental standard deviation [3] can be used to check the measure of variability in the measurement results due to the flange connection repeatability. Since the measurement results are complex quantities, the standard deviation computation is applied separately to both the real and imaginary parts of the complex-valued measured reflection coefficient.

If Γ is complex-valued measured reflection coefficient and Γ_R and Γ_I are its real and imaginary components respectively, then Γ can be written as follows:

$$\Gamma = \Gamma_R + j\Gamma_I \tag{4.1}$$

where $j^2 = -1$. For n repeated measurements of Γ, the mean value of Γ_R can be computed as follows:

$$\bar{\Gamma}_R = \frac{1}{n}\sum_{k=1}^{n}\Gamma_{R_k} \tag{4.2}$$

and the experimental standard deviation of Γ_R can be expressed mathematically as follows:

$$\sigma(\Gamma_R) = \sqrt{\frac{1}{n-1}\sum_{k=1}^{n}(\Gamma_{R_k} - \bar{\Gamma}_R)^2} \tag{4.3}$$

Similarly, the mean value of Γ_I can be written mathematically as follows:

$$\bar{\Gamma}_I = \frac{1}{n}\sum_{k=1}^{n}\Gamma_{I_k} \tag{4.4}$$

and the experimental standard deviation of Γ_I can be computed as follows:

$$\sigma(\Gamma_I) = \sqrt{\frac{1}{n-1}\sum_{k=1}^{n}(\Gamma_{I_k} - \bar{\Gamma}_I)^2} \tag{4.5}$$

To understand these mathematical formulations quantitatively, the VNA measurements are performed for the WR05 waveguide standards over the frequency range of 140–220 GHz. The following sections will present the measurement results for different devices under tests (DUTs). Each DUT is measured 10 times at each frequency. The $\sigma(\Gamma_R)$ and $\sigma(\Gamma_I)$ values are computed at each frequency using 10 repeated measurements of each DUT.

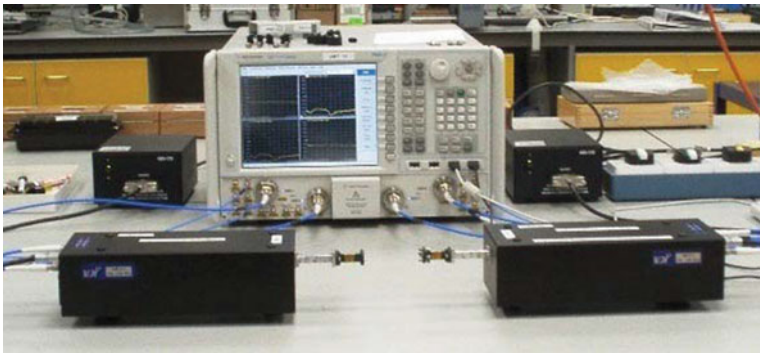

Fig. 4.1 Measurement setup used at NPL

Table 4.1 DUTs used for connection repeatability investigation

Device	Model
Flush short	*VDi*, S/N: SC 2-54
Offset short	*Flann microwave*, S/N: 177977
Matched termination	*Flann microwave*, S/N: 177714
Mismatched termination	*Flann microwave*, S/N: 177962

4.3 Experimental Setup

The measurement setup employed by National Physical Laboratory (NPL) is a four-port Agilent Technologies PNA-X network analyzer, model N5247A, covering the frequency range from 10 MHz to 67 GHz. Two *Virginia Diodes, Inc.* (VDi) WR 5.1 mm-wave extenders, VNAX239 and VNAX240, are used to extend the measurement frequency range to 140–220 GHz. Measurements are carried out in a shielded room with controlled temperature and relative humidity. The measurement setup is shown in Fig. 4.1.

The VNA is calibrated using a one port Short-Open-Load (SOL) calibration technique [4–8]. In waveguide environment, there is no open standard due to radiation effect at the open end of the waveguide, therefore offset short is used as a possible realization for the open standard. The model of calibration kit used is *VDi* WR-5.1. The one port devices under test (DUTs) used are shown in Table 4.1.

4.4 Measurement Results

The experimental standard deviation computations of the measurement results for each DUT are presented here. The standard deviation is computed separately for both real and imaginary parts of the complex-valued measured reflection coefficients.

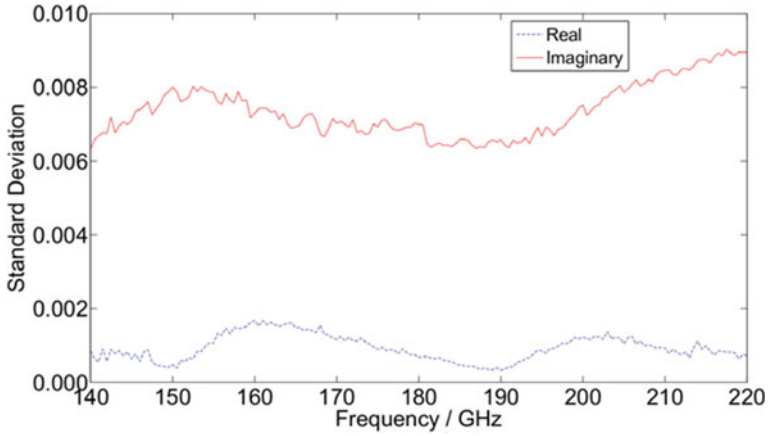

Fig. 4.2 $\sigma(\Gamma_R)$ and $\sigma(\Gamma_I)$ values for the flush short-circuit

Table 4.2 $\sigma(\Gamma_R)$ and $\sigma(\Gamma_I)$ values for the flush short-circuit at selected frequencies

Frequency (GHz)	$\sigma(\Gamma_R)$	$\sigma(\Gamma_I)$
140	0.0009	0.0063
160	0.0017	0.0073
180	0.0007	0.0070
200	0.0012	0.0075
220	0.0007	0.0090
Average	0.0010	0.0074

4.4.1 Flush Short-Circuit Measurements

The computed values of $\sigma(\Gamma_R)$ and $\sigma(\Gamma_I)$ for the flush short-circuit are shown in Fig. 4.2. Some selected values, taken at equally spaced frequencies, are also presented in Table 4.2.

4.4.2 Offset Short-Circuit Measurements

The computed values of $\sigma(\Gamma_R)$ and $\sigma(\Gamma_I)$ for the offset short-circuit are shown in Fig. 4.3. Some selected values, taken at equally spaced frequencies, are also presented in Table 4.3.

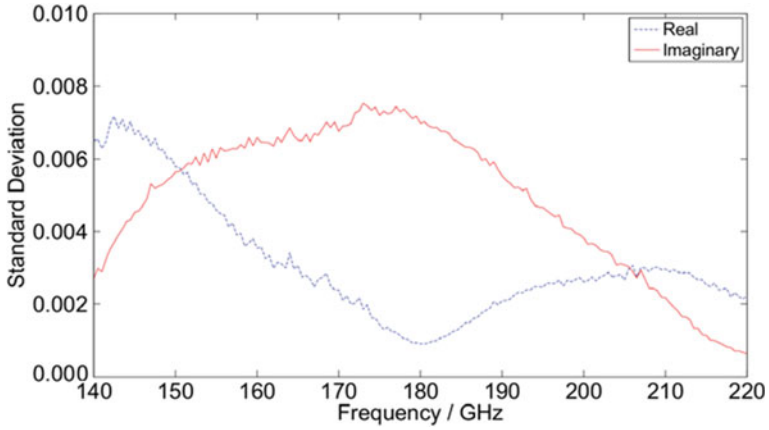

Fig. 4.3 $\sigma(\Gamma_R)$ and $\sigma(\Gamma_I)$ values for the offset short-circuit

Table 4.3 $\sigma(\Gamma_R)$ and $\sigma(\Gamma_I)$ values for the offset short-circuit at selected frequencies

Frequency (GHz)	$\sigma(\Gamma_R)$	$\sigma(\Gamma_I)$
140	0.0065	0.0027
160	0.0035	0.0066
180	0.0009	0.0070
200	0.0026	0.0038
220	0.0022	0.0006

4.4.3 Near-Matched Termination Measurements

The computed values of $\sigma(\Gamma_R)$ and $\sigma(\Gamma_I)$ for near-matched termination are shown in Fig. 4.4. Some selected values, taken at equally spaced frequencies, are also presented in Table 4.4.

4.4.4 Mismatched Termination Measurements

The computed values of $\sigma(\Gamma_R)$ and $\sigma(\Gamma_I)$ for mismatched termination are shown in Fig. 4.5. Some selected values, taken at equally spaced frequencies, are also presented in Table 4.5.

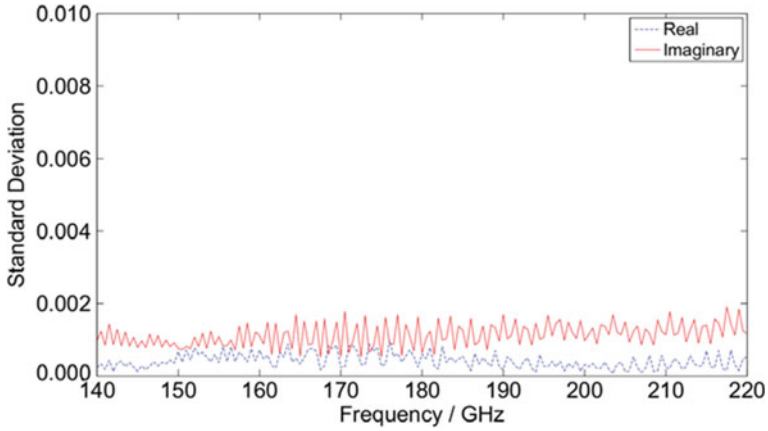

Fig. 4.4 $\sigma(\Gamma_R)$ and $\sigma(\Gamma_I)$ values for the near-matched termination

Table 4.4 $\sigma(\Gamma_R)$ and $\sigma(\Gamma_I)$ values for the near-matched termination at selected frequencies

Frequency (GHz)	$\sigma(\Gamma_R)$	$\sigma(\Gamma_I)$
140	0.0002	0.0010
160	0.0007	0.0011
180	0.0006	0.0007
200	0.0003	0.0010
220	0.0005	0.0012
Average	0.0005	0.0010

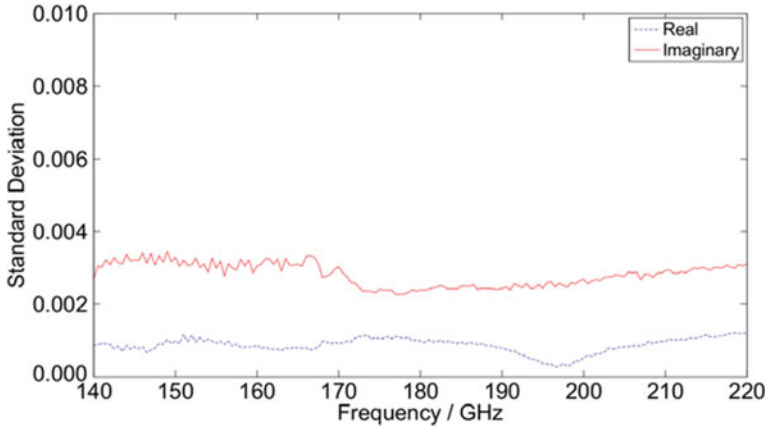

Fig. 4.5 $\sigma(\Gamma_R)$ and $\sigma(\Gamma_I)$ values for the mismatched termination

Table 4.5 $\sigma(\Gamma_R)$ and $\sigma(\Gamma_I)$ values for the mismatched termination at selected frequencies

Frequency (GHz)	$\sigma(\Gamma_R)$	$\sigma(\Gamma_I)$
140	0.0009	0.0027
160	0.0009	0.0031
180	0.0010	0.0024
200	0.0005	0.0027
220	0.0012	0.0031
Average	0.0009	0.0028

4.5 Discussions

The trend of the experimental standard deviations vary considerably among each of the four DUTs. In the case of the flush short-circuit, the trend of the experimental standard deviation does not show much variation with frequency in both real and imaginary components of the measured reflection coefficient. The same is true for near-matched termination and the mismatched termination. However, the experimental standard deviation vary considerably with frequency in both real and imaginary components of the measured reflection coefficient for the offset short-circuit. The trend is due to the variation in reflection coefficient phase with frequency as shown in Fig. 4.6. This phase variation is due to the offset length of the offset short-circuit. It is observed that as the reflection coefficient phase passes through zero degrees, the experimental standard deviation of the real part reaches a minimum and the one of the imaginary part reaches a maximum (see Fig. 4.3). It can also be seen that the ratio between the experimental standard deviation in the real component to the standard

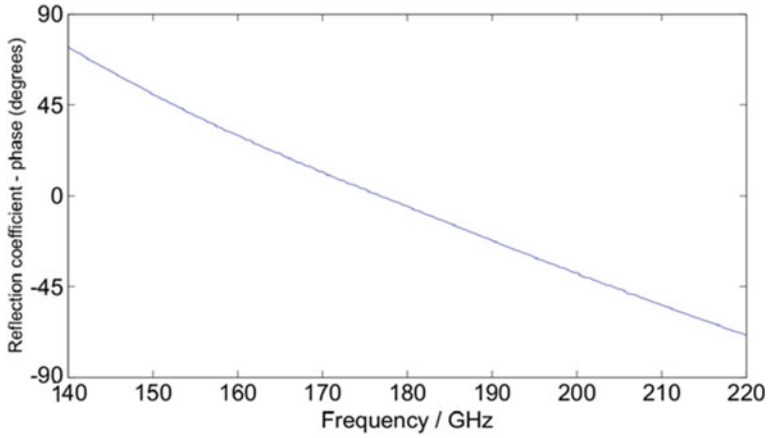

Fig. 4.6 Measured phase of the offset short-circuit

deviation in the imaginary component goes to 1 when the reflection coefficient phase is near to either $+45^\circ$ or -45°.

In case of flush short-circuit, the standard deviation in imaginary component is approximately seven times larger than the standard deviation in real component. For near-matched termination, the standard deviation in imaginary component is approximately twice larger than the standard deviation in real component. For mismatched termination, the standard deviation in imaginary component is approximately three times larger than the standard deviation in real component. In all three cases, an ellipse will be needed to enclose the scatter of the measurement values of this DUT, the size and orientation of which would remain relatively constant with respect to the frequency.

Finally, for offset short-circuit, the ratio of the standard deviation in imaginary component to the standard deviation in real component vary considerably with respect to the frequency. Therefore, even though an ellipse will be needed to enclose the scatter of the measurement values of this DUT, but the size and orientation of this ellipse would vary considerably with respect to the frequency.

4.6 Conclusion

This chapter presented the flange connection repeatability investigation of the VNA in WR05 waveguide standards over the frequency band 140–220 GHz. Four devices are used in the investigation: a flush short-circuit, an offset short-circuit, a near-matched termination and a mismatched termination. The repeatability analysis is based on the computation of experimental standard deviation of repeated measurements at each frequency for each DUT in order to highlight the measurement data variability. This analysis is performed separately for both real and imaginary components of the measured complex-valued reflection coefficient. The typical values of the experimental standard deviation observed for each DUT are: ≤ 0.001 for the near-matched termination; ≤ 0.003 for the mismatched termination; ≤ 0.007 for the offset short-circuit and ≤ 0.008 for the flush short-circuit.

This connection repeatability investigation highlighted the importance of waveguide flange alignment mechanisms for accurate VNA measurements at millimeter frequencies. The same analysis can be carried out for other frequency bands as well. The repeatability results can be subsequently used as one of the uncertainty contributions while evaluating the complete uncertainty for the VNA measurements.

References

1. Shoaib N, Ridler NM, Salter MJ (2015) "Commissioning of the NPL WR-05 Waveguide Network Analyser System for S-parameter Measurements from 140 GHz to 220 GHz", NPL Report TQE 12, ISSN: 1754–2995. National Physical Laboratory, UK, pp 1–29

2. JCGM 200:2012 " International vocabulary of metrology basic and general concepts and associated terms", 3rd edn, 2012. www.bipm.org
3. BIPM, IFCC, ILAC, ISO, IUPAC, IUPAP and OIML, "JCGM 100:2008, evaluation of measurement data - Guide to the expression of uncertainty in measurement", International Organization for Standardization (ISO), Sep. 2008 [Online]. http://www.bipm.org/en/publications/guides/gum.html
4. Kruppa W, Sodomsky KF (1971) "An explicit solution for the scattering parameters of a linear two-port measured with an imperfect test set", IEEE Trans. Microwave Theory Tech. MTT-19(1), pp 122–123
5. Rehnmark S (1974) On the calibration process of automatic network analyzer systems. IEEE Trans. Microwave Theory Tech. 22(4):457–458
6. Engen GF (1974) "Calibration technique for automated network analyzers with application to adapter evaluation", IEEE Trans. Microwave Theory Tech. MTT-22:1255–1260
7. Franzen NR, Speciale RA (1975) "A new procedure for System Calibration and error removal in automated Sparameter measurements", In: Proceedings of the 5th European Microwave Conference (Hamburg) pp 69–73
8. Fitzpatrick J (1978) Error models for system measurement. Microwave Journal 21:63–66

Chapter 5
VNA Verification Artefacts

Abstract The performance of the VNA systems is necessary to verify in order to achieve accurate measurements and traceability to the International System of Units (SI). This chapter will present the suitable verification artefacts to verify the performance of the VNAs including their applicability to coaxial and waveguide systems. The transmission loss errors of the verification artefacts, due to the dimensional tolerances and the flange misalignments, will also be discussed.

5.1 Introduction

Over the past few years, the VNA instrumentation is introduced to perform the waveguide measurements at frequencies of several hundreds of GHz [1]. In waveguide systems, such verification at lower frequencies is carried out using the precision and reduced height waveguide sections. However, at higher millimetre and submillimetre wavelengths, it is mechanically challenging to manufacture the high precision waveguide sections with reduced height because of the small dimensions required for the conventional waveguide aperture. Currently, the verification devices for measurements above 110 GHz are either not available or lack in traceability to the SI.

In last couple of years, cross-guide devices were introduced as verification standards for measurements at frequencies of above 110 GHz. The cross-guide device is a precision waveguide section (shim) that is connected in such a way that its aperture is at right angles to the apertures of the conventionally connected waveguides (i.e. VNA test port reference planes). These devices provide significant transmission losses and can be employed as verification standards [2–7]. The cross-guides can be used as calculable verification standards at different waveguide frequency bands [7]. However when using the cross-guides, the precision dowel holes of the conventional UG-387 flange are no longer usable. On the other hand, a shim consisting of a circular iris shows the same behaviour of the cross-guides, with the advantage that it is possible to use precision holes too. Moreover, the circular iris section are relatively easy to manufacture as compare to cross-guides. Therefore, the custom made circular iris can also be used as verification standards, since they also provide signifi-

N. Shoaib, *Vector Network Analyzer (VNA) Measurements and Uncertainty Assessment*, PoliTO Springer Series, DOI 10.1007/978-3-319-44772-8_5

cant transmission losses when connected to conventional rectangular waveguide test ports [4]. In this way, both the cross-guide and the circular iris sections are the candidates for the attenuation standards to verify the performance of the VNAs operating at frequencies above 110 GHz. In this chapter the characterization of cross-guides and circular iris section is carried by taking into account the dimensional tolerances as well as the flange misalignment. The dimensional tolerances include the height, width, length and corner radii tolerances for cross-guides and diameter and length tolerances for circular iris section. The flange misalignment information includes the flange height, width and the connection angle misalignments. The different uncertainty sources due to dimensional tolerances and flange misalignment are computed using the electromagnetic theory according to the parametric information given in IEEE std 1785.1-2012 standard [8] and in IEEE std 1785.2-2014 standard [9]. The dimensional tolerances are suggested in IEEE std 1785.1-2012 standard [8]. The flange misalignment for cross-guides are derived from the specifications of an UG-387 waveguide flange [10], while the flange misalignment for circular iris are derived from the values suggested in IEEE std 1785.2-2014 standard [9]. The waveguide verification standards considered for analysis are: WR-05 (140–220 GHz) and WR-03 (220–325 GHz) cross-guides and a custom-made WR-03 (220–325 GHz) circular iris section [11, 12].

In addition to the waveguide verification standards, the coaxial verification standard is also presented. A novel type N coaxial verification standard architecture (DC-18 GHz) based on an air-line is designed, fabricated and analyzed. This coaxial architecture is a relatively simple model if compared to already existing attenuation standards which are based on T- or π-network configurations of lumped elements (e.g. [13]). The simple approach enables the realization of a calculable standard. The measurement uncertainties are computed by taking into account the dimensional and dielectric tolerances [14, 15].

All the data analysis is carried out in complex domain i.e., for real and imaginary values of scattering parameters (S-parameters). The measurement uncertainty due to different error sources is computed according to the *Law of Propagation of Uncertainty* [16]. The real and imaginary data along with the associated uncertainty are converted in magnitude and phase representation by linear propagation of uncertainties taking into account the correlation between real and imaginary part of the S-parameters [17]. The electromagnetic computations are performed using an electromagnetic simulation software, namely, Computer Simulation Technology (CST) Microwave Studio [18]. The experimental results are compared with the electrical performance predicted using the CST Microwave Studio software.

5.2 Dimensional Tolerances and Flange Misalignment

The transmission loss errors of the verification standards can be computed from the dimensional tolerances and the flange misalignments using the electromagnetic theory. The nominal values for cross-guide aperture height and width are used during

the simulations. The circular iris section diameter measurements are obtained by an optical method. The length measurements are carried out using a digital micrometer with measurement uncertainty of 3 μm. The grade information for cross-guide height and width tolerances are used as mentioned in IEEE std 1785.1-2012 standard [8]. In particular, the grade 0.5 with maximum voltage reflection coefficient (VRC) of −34 dB between perfectly aligned waveguides is chosen. The flange misalignment data are obtained from IEEE std 1785.2-2014 standard [9]. The connection angle tolerance is derived from the specifications for a conventional UG-387 waveguide flange [10]. The flange misalignment for circular iris section are derived from the values suggested in IEEE std 1785.2-2014 standard [9]. The dimensional tolerances and the flange misalignments for cross-guides and circular iris section are shown in Table 5.1.

Table 5.1 Cross-guides and circular iris section tolerances and the flange misalignment

Cross-guides									
Standard name	Nominal width a/μm	Nominal height b/μm	Length $l_w/\mu m$	Dimensional tolerances/μm			Flange misalignments/μm		
				Width Δa_w	Height Δb_w	Length Δl_w	Width Δa_{fl}	Height Δb_{fl}	Connection Angle/^{o} $\Delta\Theta$
WR-05	1295	647.5	0.9890	6.5	6.5	3	150	150	1.2
WR-03	864	432.0	0.9830	4.3	4.3	3	150	150	1.2
Circular iris section									
	Diameter $d_w/\mu m$			Diameter Δd_w					
WR-03	499		0.9084	4.3		3	19	14	0.3

Table 5.2 Tolerances for type N coaxial verification standard

Mechanical tolerances		
Parameter	Value/mm	Tolerance/μm
Outer conductor diameter (d_{out})	7.00	10
Inner conductor diameter (d_{in})	3.04	10
Inner cylindrical holes diameter (d_h)	1.57	10
Cylindrical dielectric material diameter [$1^{st} Topology$] (d_{in})	3.04	10
Cylindrical dielectric material diameter [$2^{nd} Topology$] (d_{out})	7.00	10
Inner conductor sections length (l_1)	16.73	10
Below cut-off section length (l_2)	4.00	10
Inner cylindrical holes length (l_3)	3.00	10
Dielectric material inner cylinders length (l_4)	2.50	10
Dielectric tolerance		
Parameter	Value	Tolerance
Teflon (PTFE) epsilon (ϵ_r)	2.1	±0.1

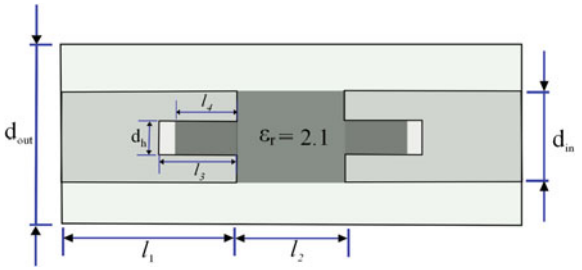

Fig. 5.1 Coaxial verification standard using the below cut-off section (1^{st} Topology) (Side View)

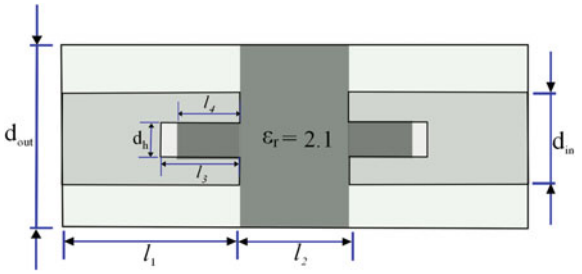

Fig. 5.2 Coaxial verification standard using the below cut-off section (2^{nd} Topology) (Side View)

The dimensional measurements for the type N coaxial verification standard have also been carried out. The diameters of inner and outer conductor of the coaxial standard are obtained using a mechanical setup composed of micrometers. The length measurements are carried out using using a digital micrometer. The dimensional and dielectric tolerances for coaxial verification standard are shown in Table 5.2. The permittivity data for a polytetrafluoroethylene (PTFE) section, obtained from the material data sheet, is also given. The side cross-sectional views for the coaxial verification standard for the two topologies, highlighting the different parameters, are shown in Figs. 5.1 and 5.2.

5.3 Electromagnetic Simulations

The electromagnetic characteristics of the cross-guides, circular iris section and the coaxial verification standard have computed using the time domain solver in CST Microwave Studio software. Simulation results using frequency domain solver showed negligible differences. The electromagnetic characteristics are defined in terms of complex S-parameters (more specifically the transmission S-parameters) and calculated from the nominal values of dimensions of the artefact along with the dimensional tolerances and flange misalignments. In the following subsections,

an overview of electromagnetic simulations for waveguide and coaxial artefacts is presented.

5.3.1 *Electromagnetic Simulations for Waveguide Artefacts*

In the computational domain, the background material is set to perfectly electrical conductor (PEC). The vacuum bricks are used to define the waveguide flange and the cross-guides connected between the two flanges. On the other hand, the vacuum cylinders are used to define the circular iris section. The diagrams illustrating the cross-guide and the circular iris section connection strategy for WR-03 waveguide standard (as an example) are shown in Figs. 5.3 and 5.4 respectively. The waveguide ports at the inputs of the waveguide flange sections are defined for energy feeding and extraction from the computational domain. The hexahedral mesh type is used for

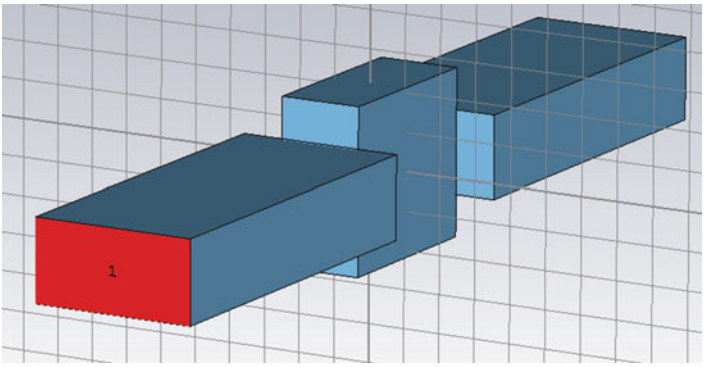

Fig. 5.3 WR-03 cross-guide connection strategy in CST Microwave Studio

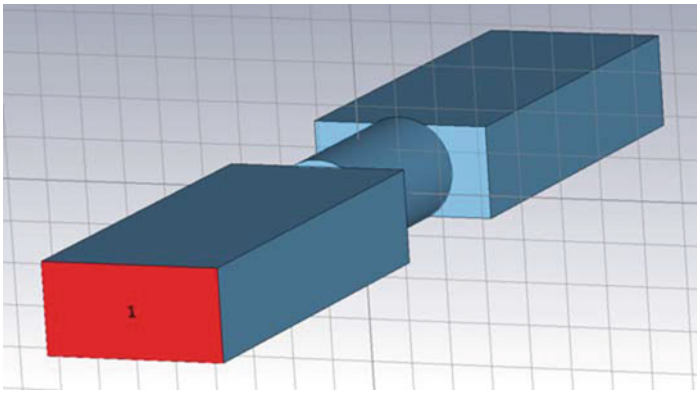

Fig. 5.4 WR-03 circular iris section connection strategy in CST Microwave Studio

computational domain discretization. The S-parameters of cross-guide or circular iris section alone are computed by de-embedding procedure in which the reference plane is shifted from the waveguide ports to the cross-guide or circular iris section ports. This de-embedding procedure only affected the phase of the S-parameters because all the waveguides are assumed to be lossless during the simulations.

The transmission loss errors for cross-guides and circular iris section are computed using the dimensional tolerances and the flange misalignments shown in Table 5.1. The corner radii of the waveguide aperture are assumed to have negligible influence on transmission loss computations, therefore, their influences have not been included in the simulations. The complex S-parameter data obtained from CST Microwave Studio have then been exported into touch-stone format for post processing. The post processing is performed in the numerical computing environment MATLAB [19]. In MATLAB, all the complex data along with uncertainty are transformed into the magnitude and phase format with their respective uncertainty for graphical representation.

5.3.2 Electromagnetic Simulations for Coaxial Artefact

A novel type N coaxial verification standard (DC-18 GHz) based on an air-line is simulated. In order to achieve significant transmission losses, a below cut-off section is used by cutting the inner cylindrical conductor of the coaxial air-line in two halves. The gap between the halves as a below cut-off section. This gap is filled with a cylindrical dielectric inset. The two halves together with dielectric inset act as a capacitor. Two different topologies are considered for the verification standard. In first topology, the diameter of the cylindrical dielectric inset is set equal to the diameter of the inner cylindrical conductor, while in second topology, the diameter of the cylindrical inset is set equal to the outer cylindrical conductor of the coaxial air-line. The latter configuration is advantageous because it provides much better stability in aligning the two halves with the longitudinal axis of the coaxial standard. The diagrams illustrating the inner conductor simulation models for the two configurations of coaxial verification standard are shown in Figs. 5.5 and 5.6. The side cross-sectional views for both configurations are also shown in Figs. 5.1 and 5.2. The side views highlight the

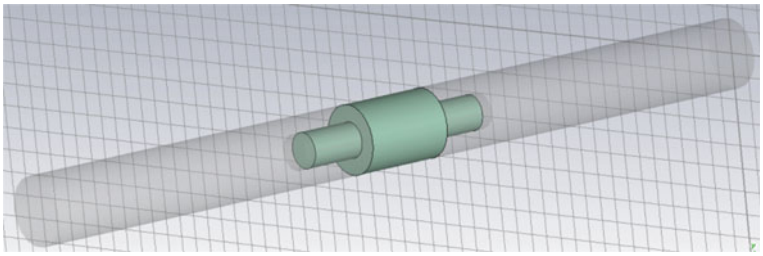

Fig. 5.5 Inner conductor simulation model of coaxial verification standard (1^{st} Topology)

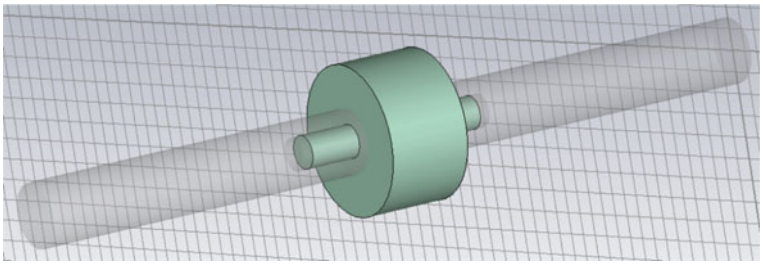

Fig. 5.6 Inner conductor simulation model of coaxial verification standard (2^{nd} Topology)

dimensional parameters for which the tolerances are shown in Table 5.2. The background material is set to perfectly electrical conductor (PEC). The vacuum cylinders are used to define the inner and outer cylindrical conductors of the coaxial air-line as well as the cylindrical dielectric section. The waveguide ports at the inputs of the two halves are defined for energy feeding and extraction from the computational domain. The hexahedral mesh type is used for computational domain discretization. The dielectric material considered for the verification standard is PTFE (Teflon). The transmission loss errors are computed using the dimensional and dielectric tolerances shown in Table 5.2. The complex S-parameter data obtained from CST Microwave Studio results have then been exported into touch-stone format for post processing in MATLAB.

5.4 Uncertainty Estimation

The performance of the cross-guides, circular iris section and coaxial standard, as transmission loss verification standard, can be specified in terms of uncertainty due to dimensional tolerances and the flange misalignments shown in Tables 5.1 and 5.2. The measurement uncertainty due to different error sources is computed according to the *Law of Propagation of Uncertainty* [16]. The real and imaginary data along with the associated uncertainty are converted in magnitude and phase representation by linear propagation of uncertainties [17].

If $S = x + jy$ denotes the complex transmission S-parameter, then for cross-guide verification standard, the mathematical equations used to define the combined standard uncertainty for the S-parameter can be written, in terms of dimensional tolerance and flange misalignment parameters shown in Table 5.1, as:

$$u(x) = \sqrt{\underbrace{\left(\frac{\partial x}{\partial a_w}\right)^2\left(\frac{\Delta a_w}{\sqrt{3}}\right)^2}_{(u(\Delta a_w))^2} + \underbrace{\left(\frac{\partial x}{\partial b_w}\right)^2\left(\frac{\Delta b_w}{\sqrt{3}}\right)^2}_{(u(\Delta b_w))^2} + \underbrace{\left(\frac{\partial x}{\partial l_w}\right)^2\left(\frac{\Delta l_w}{\sqrt{3}}\right)^2}_{(u(\Delta l_w))^2} \ldots} \\ \sqrt{\underbrace{+\left(\frac{\partial x}{\partial a_{fl}}\right)^2\left(\frac{\Delta a_{fl}}{\sqrt{3}}\right)^2}_{(u(\Delta a_{fl}))^2} + \underbrace{\left(\frac{\partial x}{\partial b_{fl}}\right)^2\left(\frac{\Delta b_{fl}}{\sqrt{3}}\right)^2}_{(u(\Delta b_{fl}))^2} + \underbrace{\left(\frac{\partial x}{\partial \Theta}\right)^2\left(\frac{\Delta \Theta}{\sqrt{3}}\right)^2}_{(u(\Delta \Theta))^2}}, \tag{5.1}$$

and

$$u(y) = \sqrt{\underbrace{\left(\frac{\partial y}{\partial a_w}\right)^2\left(\frac{\Delta a_w}{\sqrt{3}}\right)^2}_{(u(\Delta a_w))^2} + \underbrace{\left(\frac{\partial y}{\partial b_w}\right)^2\left(\frac{\Delta b_w}{\sqrt{3}}\right)^2}_{(u(\Delta b_w))^2} + \underbrace{\left(\frac{\partial y}{\partial l_w}\right)^2\left(\frac{\Delta l_w}{\sqrt{3}}\right)^2}_{(u(\Delta l_w))^2} \ldots} \\ \sqrt{\underbrace{+\left(\frac{\partial y}{\partial a_{fl}}\right)^2\left(\frac{\Delta a_{fl}}{\sqrt{3}}\right)^2}_{(u(\Delta a_{fl}))^2} + \underbrace{\left(\frac{\partial y}{\partial b_{fl}}\right)^2\left(\frac{\Delta b_{fl}}{\sqrt{3}}\right)^2}_{(u(\Delta b_{fl}))^2} + \underbrace{\left(\frac{\partial y}{\partial \Theta}\right)^2\left(\frac{\Delta \Theta}{\sqrt{3}}\right)^2}_{(u(\Delta \Theta))^2}}, \tag{5.2}$$

where, for example, $\left(\frac{\partial x}{\partial a_w}\right)$ is the sensitivity coefficient and describes how the real part of S-parameter, x, varies with corresponding small tolerance in waveguide width a_w. The parameter, $u(\Delta a_w)$, represents the equivalent standard uncertainty due to a_w. For circular iris section, the width tolerance a_w and height tolerance b_w are replaced by the waveguide diameter tolerance d_w. Similarly, in case of coaxial verification standard, the above equations can be rewritten in terms of dimensional tolerances shown in Table 5.2.

The real and imaginary S-parameter data along with the uncertainty is used to compute the uncertainty of magnitude and phase quantities of S-parameters according to the Eqs. 1.43 and 1.44 already discussed in Chap. 1- Sect. 1.4. The expanded uncertainty is computed by multiplying the standard uncertainty with coverage factor $k = 2$. The propagation of uncertainty from real and imaginary to magnitude and phase quantities is carried out using the *LinProp* module, developed by *Bundesamt für Metrologie (METAS)* [20], whose definition is based on *GUM Tree* algorithm [21–23]. This module is directly accessible in MATLAB. The data obtained using the CST Microwave Studio simulations are complex quantities. There exists a correlation between the real and imaginary parts of the complex quantity. The correlation also exists between different complex quantities. The *LinProp* module takes into account both the variance of the complex quantity and the covariance between real and imaginary parts of same complex quantity and between two different complex quantities to compute the final uncertainties in magnitude and phase.

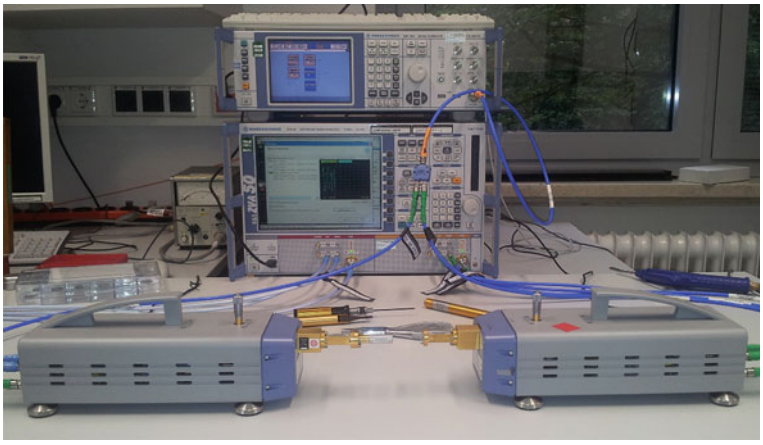

Fig. 5.7 WR-03 waveguide measurement setup used at PTB

5.5 Experimental Setup

The measurement setup employed by Physikalisch-Technische Bundesanstalt (PTB) is a two-port Rohde & Schwarz (R&S) ZVA-50 VNA, covering the frequency range from 10 MHz to 50 GHz. Measurements are carried out in a shielded room that has stable room temperature and the relative humidity.

The measurements in waveguide test setup are performed in WR-05 (140–220 GHz) and WR-03 (220–325 GHz) standards. Two R&S ZVA-Z220 millimeter-wave extenders are used to extend the measurement frequency range to 140–220 GHz while two R&S ZVA-Z325 extenders are used for measurements in the range 220–330 GHz. As an example, the measurement setup for WR-03 waveguides is shown in Fig. 5.7. The raw data of standards and the devices under test (DUTs) are collected using the VNA and an offline two port Line-Reflect-Line (LRL) calibration technique [24] is performed to obtain the corrected data. Compared to the widely used Thru-Reflect-Line (TRL) calibration technique [25], the LRL calibration technique replaces the thru standard of zero length with a line standard of non-zero length. The difference between the length of the two lines determines the effective bandwidth of the calibration procedure.

For coaxial measurements, the unknown thru calibration technique [26] with sliding load is used to calibrate the VNA in order to obtain the corrected data from the measured raw data of the standards and the DUTs. The PTB coaxial measurement setup is shown in Fig. 5.8. The DUTs are the two type N coaxial verification standards.

5.6 Results and Discussions

The simulation and measurement results for waveguide and coaxial verification artefacts are presented here. The coverage factor k = 2 is used to obtain the expanded uncertainty. The uncertainty budgets containing the different error sources are also presented. In the following subsections, the results for cross-guides, circular iris section and coaxial verification standards are discussed separately.

5.6.1 Waveguide Verification Standards

The waveguide verification standards include the cross-guides and circular iris section. The transmission loss magnitude and phase results along with combined expanded uncertainty are presented here.

Cross-Guide Verification Standards

The cross-guide verification standards measured include the WR-05 (140–220 GHz) waveguide of length 0.9890 mm and WR-03 (220–330 GHz) waveguide of length 0.9830 mm. The measured transmission magnitude and phase as function of frequency and the simulated values along with uncertainty predicted using the CST Microwave Studio software for WR-05 cross-guide of length 0.9890 mm are shown in Figs. 5.9 and 5.10. The measured transmission magnitude and phase values agreed with the simulated values within the uncertainty interval i.e., the measured values fall within the uncertainty intervals of the modeled values. The tolerances in dimensions and the flange misalignments are the sources of transmission loss errors. The simulated transmission loss errors (both in magnitude and phase) are also presented in tabular form for some selected frequencies. In practice, the transmission loss errors are computed at each frequency, even though only the results of some selected frequencies are shown in Tables 5.3 and 5.4 for WR-05 cross-guide. It can be seen from

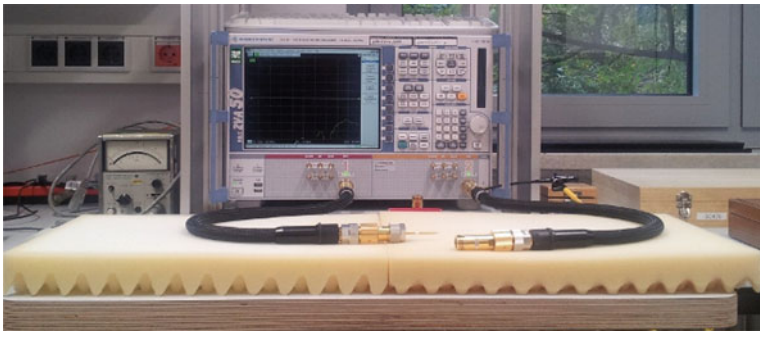

Fig. 5.8 Coaxial measurement setup used at PTB

Table 5.3 Loss errors and standard uncertainty (Std. Unc.) for WR-05 cross-guide at selected frequencies for the transmission coefficient magnitude

Freq./GHz	S_{21}/dB	$\Delta S_{21}/dB$						Std. Unc.
		Δa_w	Δb_w	Δa_{fl}	Δb_{fl}	$\Delta\Theta$	Δl_w	
140	−41.3230	0.0208	0.7888	0.5919	0.1208	0.3795	0.0964	0.4649
160	−35.4600	0.0285	0.7968	0.6273	0.1471	0.0675	0.0933	0.4535
180	−30.0210	0.0297	0.8388	0.3995	0.1197	0.1132	0.0806	0.5313
200	−24.2110	0.0319	0.8935	0.1084	0.0877	0.1354	0.0648	0.5891
220	−17.5820	0.0343	0.9728	0.4109	0.0138	0.1241	0.0409	0.5955

Table 5.4 Loss errors and standard uncertainty (Std. Unc.) for WR-05 cross-guide at selected frequencies for the transmission coefficient phase

Freq./GHz	$S_{21}/^o$	$\Delta S_{21}/^o$						Std. Unc.
		Δa_w	Δb_w	Δa_{fl}	Δb_{fl}	$\Delta\Theta$	Δl_w	
140	60.1270	0.0270	0.7335	1.7449	0.1604	0.8915	0.0263	3.0318
160	47.5250	0.0160	1.2071	2.6410	0.1517	0.7790	0.0028	3.1434
180	32.7980	0.0179	1.6845	3.0456	0.2253	0.6004	0.0013	2.4107
200	15.7100	0.0314	2.3582	2.9617	0.2514	0.9937	0.0026	1.9147
220	−7.0270	0.0435	3.4691	1.0775	0.1043	1.4787	0.0089	2.9002

the values of the loss errors shown in the tables that the tolerances in cross-guide aperture height and the flange aperture width have the most significant influence while the tolerances in cross-guide aperture width and length have the least influence on the transmission magnitude and phase final uncertainties.

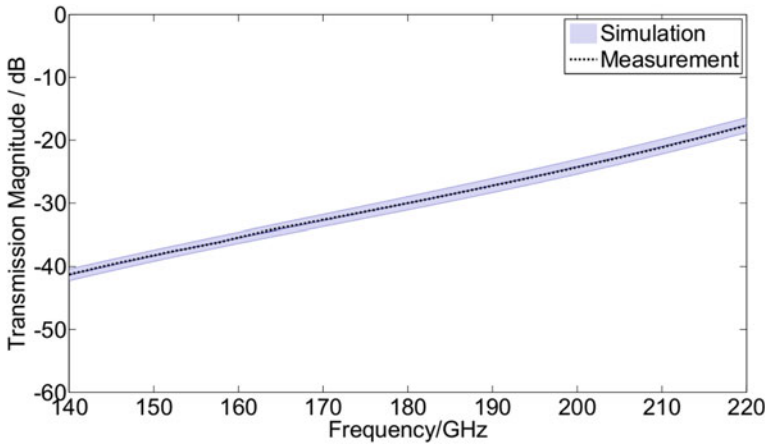

Fig. 5.9 Measurements of the transmission coefficient magnitude for a WR-05 cross-guide

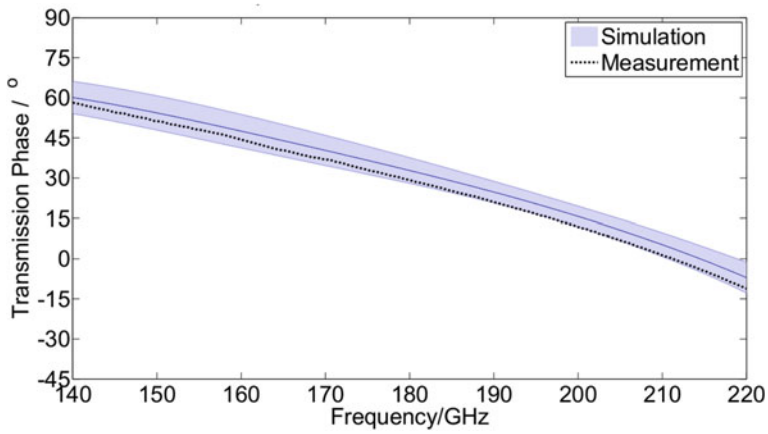

Fig. 5.10 Measurements of the transmission coefficient phase for a WR-05 cross-guide

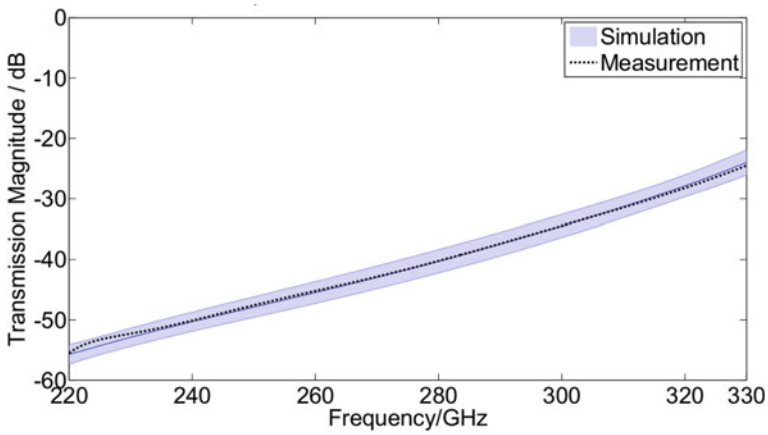

Fig. 5.11 Measurements of the transmission coefficient magnitude for a WR-03 cross-guide

Similarly, the measured and simulated transmission magnitude and phase as function of frequency for WR-03 cross-guide of length 0.9830 mm are shown in Figs. 5.11 and 5.12. The measured transmission magnitude and phase values fall within the uncertainty intervals for the modeled values. The simulated transmission loss errors (both in magnitude and phase) of some selected frequencies are also shown in Tables 5.5 and 5.6. It can be observed from the loss errors values shown in the tables that the tolerances in cross-guide aperture height and flange aperture width have the most significant influence on the transmission magnitude and phase values. On the other hand, the tolerances in cross-guide aperture width has the least influence on the transmission magnitude while the length tolerance has the least influence on the transmission phase.

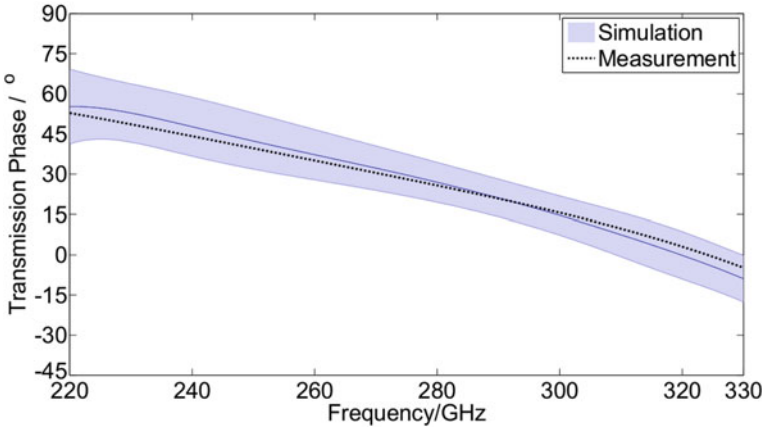

Fig. 5.12 Measurements of the transmission coefficient phase for a WR-03 cross-guide

Table 5.5 Loss errors and standard uncertainty (Std. Unc.) for WR-03 cross-guide at selected frequencies for the transmission coefficient magnitude

Freq./GHz	S_{21}/dB	$\Delta S_{21}/dB$						Std. Unc.
		Δa_w	Δb_w	Δa_{fl}	Δb_{fl}	$\Delta\Theta$	Δl_w	
220	−55.7110	0.0134	0.5767	1.7712	0.4537	0.0684	0.1587	0.8289
240	−50.2920	0.0369	1.1521	1.4224	0.3513	0.2263	0.1364	0.7964
260	−45.4590	0.0341	1.1138	1.3273	0.2126	0.0934	0.1252	0.9040
280	−40.2860	0.0349	1.2013	0.9214	0.2099	0.2218	0.1122	0.9675
300	−34.4920	0.0354	1.2999	0.5235	0.1669	0.0139	0.0947	0.9502
330	−23.9990	0.0370	1.6131	0.7112	0.0636	0.1765	0.0591	1.0470

Table 5.6 Loss errors and standard uncertainty (Std. Unc.) for WR-03 cross-guide at selected frequencies for the transmission coefficient phase

Freq./GHz	$S_{21}/^o$	$\Delta S_{21}/^o$						Std. Unc.
		Δa_w	Δb_w	Δa_{fl}	Δb_{fl}	$\Delta\Theta$	Δl_w	
220	55.2200	0.0565	0.7728	10.7280	1.2296	1.4573	0.0556	6.9800
240	47.7050	0.0202	1.0473	5.1480	0.2242	0.8900	0.0163	5.5091
260	37.2420	0.0115	1.6284	6.7267	0.7335	0.5830	0.0043	4.7043
280	26.9350	0.0249	1.7955	7.2927	0.5844	1.3750	0.0029	3.7275
300	14.6270	0.0278	2.4682	7.2670	0.7650	1.3711	0.0011	3.6400
330	−8.8870	0.0475	3.5939	4.0751	0.3197	2.0821	0.0065	4.3735

Circular Iris Verification Standard

A WR-03 (220–330 GHz) circular iris section with inner circular hole diameter of 0.499 mm has also been simulated and measured. The measured transmission magnitude and phase and the simulated values along with uncertainty predicted using the

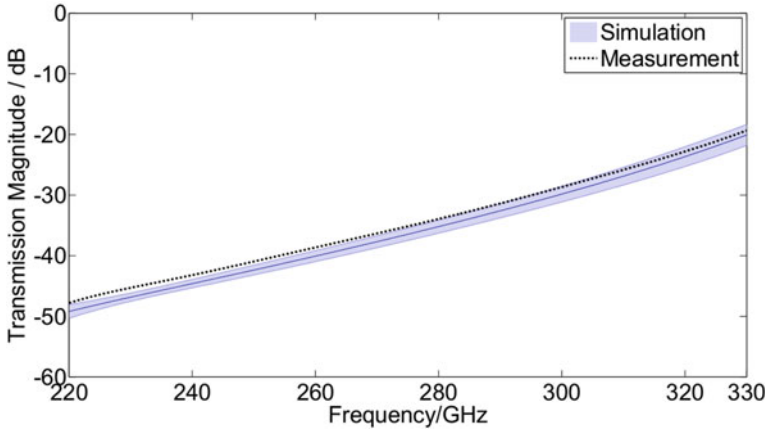

Fig. 5.13 Measurements of the transmission coefficient magnitude of a WR-03 circular iris section

Table 5.7 Loss errors and standard uncertainty (Std. Unc.) for WR-03 circular iris section at selected frequencies for the transmission coefficient magnitude

Freq./GHz	S_{21}/dB	$\Delta S_{21}/dB$					Std. Unc.
		Δd_w	Δa_{fl}	Δb_{fl}	$\Delta\Theta$	Δl_w	
220	−49.1900	1.2229	0.1860	0.2056	0.0910	0.1617	0.5694
240	−44.6010	0.8004	0.1023	0.0603	0.0307	0.1363	0.3516
260	−40.0640	1.0159	0.0171	0.0245	0.0429	0.1297	0.4553
280	−35.1980	1.0531	0.0061	0.0225	0.0447	0.1160	0.5413
300	−29.8320	1.1072	0.0025	0.0198	0.0444	0.0999	0.6509
330	−20.0790	1.3751	0.0331	0.0525	0.0476	0.0662	0.8613

CST Microwave Studio software are shown in Figs. 5.13 and 5.14. The transmission measurement results appear to be slightly outside the uncertainty intervals for the modeled transmission values at some frequency points. It should be noted that the transmission measurements also have their own uncertainty (i.e., due to VNA measurement setup). Therefore, if both modeled and measurement values along with their corresponding uncertainties will be plotted together, then there should be an overlapping of uncertainty intervals over the whole frequency band. The transmission loss errors budget tables containing both magnitude and phase errors of some selected frequencies are also shown in Tables 5.7 and 5.8. It can be seen from the loss errors values that the tolerance in circular iris section diameter has the most significant influence on the transmission magnitude and phase results. On the other hand, the tolerances in flange aperture width and length have the least influence on the transmission magnitude and phase values respectively.

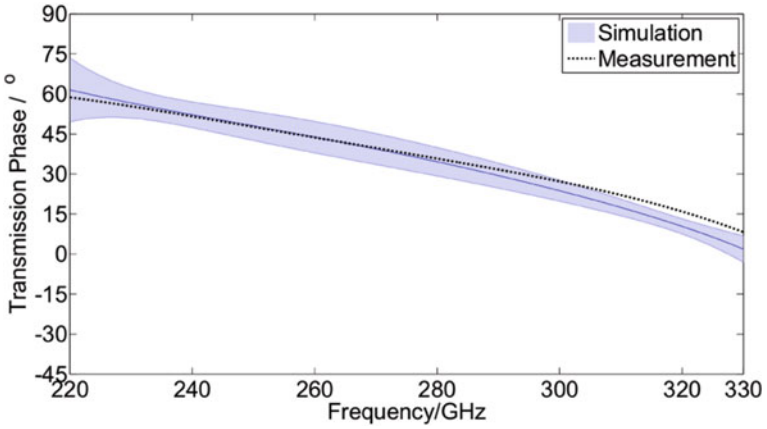

Fig. 5.14 Measurements of the transmission coefficient phase of a WR-03 circular iris section

Table 5.8 Loss errors and standard uncertainty (u) for WR-03 circular iris section at selected frequencies for the transmission coefficient phase

Freq./GHz	$S_{21}/^o$	$\Delta S_{21}/^o$					Std. Unc.
		Δd_w	Δa_{fl}	Δb_{fl}	$\Delta\Theta$	Δl_w	
220	61.5130	6.5666	3.7666	2.4639	0.7152	0.1330	6.0120
240	52.2030	1.0819	0.0714	0.0376	0.5532	0.0014	2.4148
260	43.8090	1.1548	0.1751	0.0965	0.5771	0.0044	2.9550
280	34.5890	1.8800	0.0770	0.1073	0.6792	0.0045	2.6743
300	23.7290	2.1361	0.0515	0.0460	0.7515	0.0024	1.9714
330	1.8885	3.8226	0.2233	0.3187	0.9222	0.0048	2.4712

5.6.2 Coaxial Verification Standard

The type N coaxial verification standard with both topologies are simulated and measured. The measured transmission loss magnitude and phase results and the modeled values predicted using the electromagnetic theory are presented here. For simulation results, the coverage factor k = 2 is used to obtain the expanded uncertainty. The hardware realization of coaxial verification standard with both topologies are shown in Figs. 5.15 and 5.16 and both are fabricated at PTB.

The measured transmission magnitude and phase and the simulated values along with uncertainty predicted using the CST Microwave Studio software for coaxial verification standard with both topologies are shown in Figs. 5.17, 5.18, 5.19 and 5.20. The measured transmission magnitude and phase values agreed very well to the simulated values within the uncertainty interval of the modeled values. The transmission loss errors budget tables containing both magnitude and phase errors of some selected frequencies for coaxial verification standard (with 1^{st} topology as an example) are

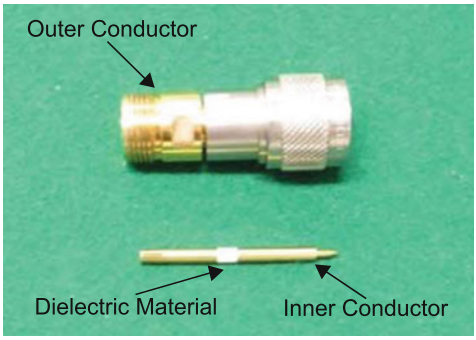

Fig. 5.15 Hardware realization of Coaxial verification standard (1^{st} Topology)

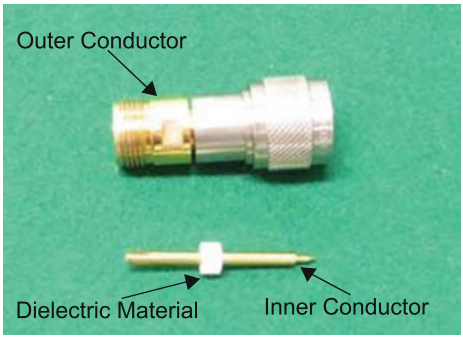

Fig. 5.16 Hardware realization of Coaxial verification standard (2^{nd} Topology)

also shown in Tables 5.9 and 5.10. It can be observed from the loss errors values that the tolerances in dielectric constant (ϵ) has the most significant influence on the transmission magnitude and phase results. On the other hand, the tolerances in inner cylindrical holes diameter (d_h) and the below cut-off section length (l_2) have the least influence on the transmission magnitude and phase values respectively. During simulations, it is observed that the tolerances in the inner conductor sections length (l_1), inner cylindrical holes length (l_3) and the dielectric material inner cylinders length (l_4) have no significant influence on transmission magnitude and therefore they have not been included in the budget table shown in Table 5.9. It has also been observed that the tolerances in inner cylindrical holes length (l_3) and the dielectric material inner cylinders length (l_4) have no significant influence on transmission phase and therefore they have also not been included in the budget table shown in Table 5.10.

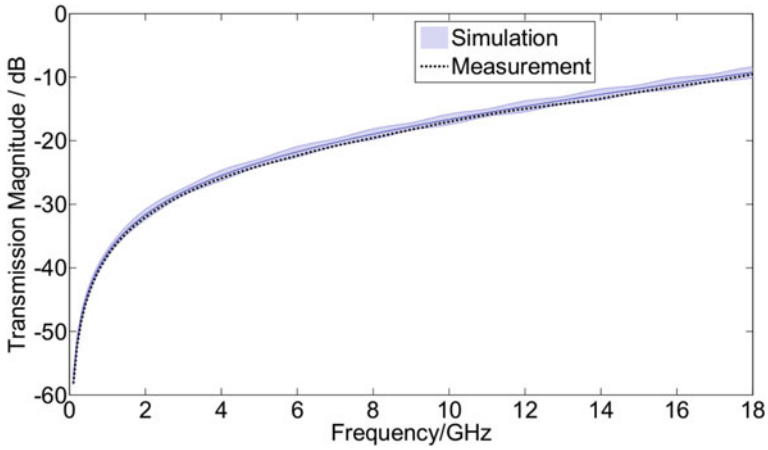

Fig. 5.17 Measurements of the transmission coefficient magnitude of Coaxial verification standard (1^{st} Topology)

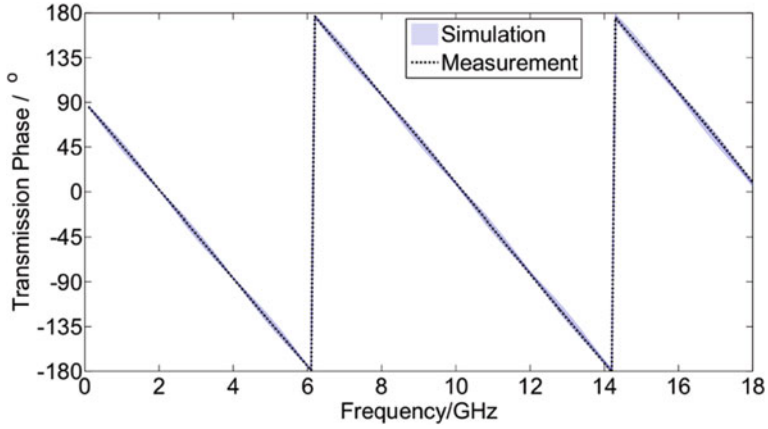

Fig. 5.18 Measurements of the transmission coefficient phase of Coaxial verification standard (1^{st} Topology)

5.7 Conclusion

This chapter presented the transmission loss magnitude and phase uncertainty analysis for waveguide and coaxial artefacts to be used as standards of attenuations. The waveguide verification artefacts include the WR-05 and WR-03 cross-guides and a WR-03 circular iris section. On the other hand, the coaxial verification artefact discussed is a novel type N coaxial verification standard based on an air-line.

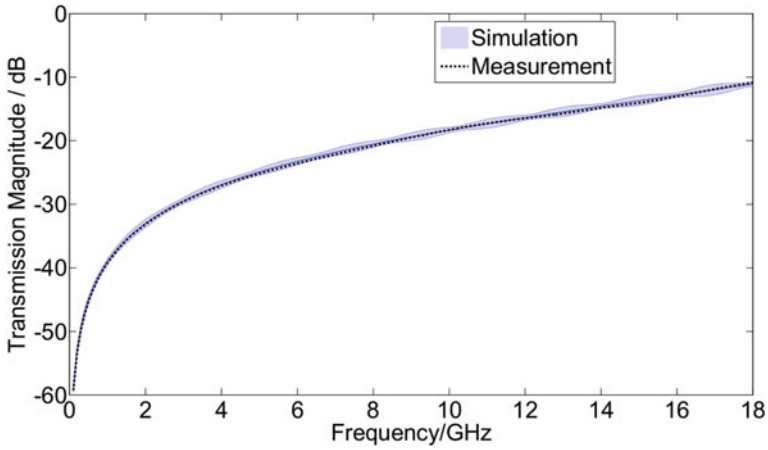

Fig. 5.19 Measurements of the transmission coefficient magnitude of Coaxial verification standard (2^{nd} Topology)

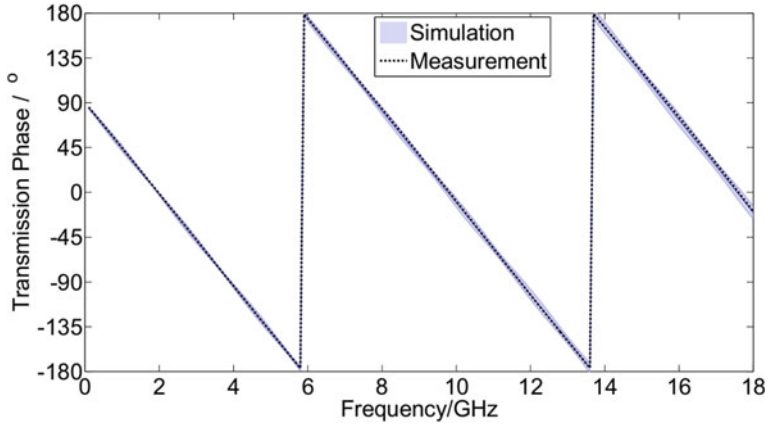

Fig. 5.20 Measurements of the transmission coefficient phase of Coaxial verification standard (2^{nd} Topology)

Table 5.9 Loss errors and standard uncertainty (Std. Unc.) for coaxial verification standard (1^{st} Topology) at selected frequencies for the transmission coefficient magnitude

Freq./GHz	S_{21}/dB	$\Delta S_{21}/dB$						Std. Unc.
		Δd_{in}	Δd_{out}	Δd_h	Δl_2	$\Delta \epsilon_{r1}$	$\Delta \epsilon_{r2}$	
1	−37.6701	0.0169	0.0318	0.0080	0.0494	0.5066	0.4844	0.2870
5	−23.4416	0.0173	0.0314	0.0081	0.0484	0.5088	0.4865	0.2885
10	−16.6365	0.0188	0.0306	0.0083	0.0450	0.5151	0.4923	0.4193
15	−11.8112	0.0211	0.0297	0.0081	0.0385	0.5197	0.4945	0.2954
18	−9.2301	0.0225	0.0284	0.0079	0.0327	0.5139	0.4860	0.4347

Table 5.10 Loss errors and standard uncertainty (Std. Unc.) for coaxial verification standard (1^{st} Topology) at selected frequencies for the transmission coefficient phase

Freq./GHz	$S_{21}/^o$	$\Delta S_{21}/^o$							Std. Unc.
		Δd_{in}	Δd_{out}	Δd_h	Δl_1	Δl_2	$\Delta \epsilon_{r1}$	$\Delta \epsilon_{r2}$	
1	45.9904	0.0006	0.0103	0.0055	0.0157	0.0006	0.0789	0.0815	1.8940
5	−130.3900	0.0040	0.0780	0.0220	0.0849	0.0040	0.4130	0.4060	1.9296
10	8.1772	0.0127	0.1567	0.0461	0.1698	0.0069	0.8804	0.8706	0.5255
15	144.3200	0.0310	0.2400	0.0720	0.2546	0.0070	1.4840	1.4720	2.2785
18	8.0447	0.0494	0.2953	0.0880	0.3058	0.0026	1.9475	1.9279	1.2705

The effects on the verification artefacts transmission magnitude and phase due to the dimensional tolerances and flange misalignments are predicted using the electromagnetic modeling with the CST Microwave Studio software. The model-based measurement uncertainty due to different error sources is computed according to the *Law of Propagation of Uncertainty*. The measured values resulted to be in good agreement with the simulated values within the model-based uncertainty intervals. From the analysis presented here, it can be concluded that the performance of the VNAs operating at millimeter wavelengths can be verified using the cross-guides and the circular iris section. Also, the type N coaxial verification artefact presented can also be used as a verification standard in the frequency range of DC-18 GHz.

References

1. Adamson D, Ridler NM, Howes J (2009) Recent and future developments in millimetre and sub-millimetre wavelength measurement standards at NPL. In: 5th ESA workshop on millimetre wave technology and applications and 31st ESA antenna workshop, Netherlands, pp 463–467
2. Ridler N, Salter MJ (2013) Cross-connected waveguide lines as standards for millimeter- and submillimeter-wave vector network analyzers. In: 81st ARFTG microwave measurement conference (ARFTG), 2013, pp 1–7
3. Ridler NM, Clarke RG, Salter MJ, Wilson A (2010) Traceability to national standards for S-parameter measurements in waveguide at frequencies from 140 GHz to 220 GHz. In: Proceedings of the 76th ARFTG microwave measurement conference, Clearwater Beach, FL, pp

1–7
4. Schrader T, Kuhlmann K, Dickhoff R, Dittmer J, Hiebel M (2011) Verification of scattering parameter measurements in waveguides up to 325 GHz including highly-reflective devices. Adv Radio Sci 9:9–17
5. Ridler NM, Clarke R, Salter MJ, Wilson A (2013) The trace is on measurements: developing traceability for S-parameter measurements at millimeter and submillimeter wavelengths. IEEE Microw Mag 14(7):67–74
6. Huang H, Ridler NM, Salter MJ (2014) Using electromagnetic modeling to evaluate uncertainty in a millimeter-wave cross-guide verification standard. In: 83rd ARFTG microwave measurement conference (ARFTG), Tampa, Florida, USA
7. Salter MJ, Ridler NM (2014) Use of reduced aperture waveguide as a calculable standard for the verification of millimetre-wave vector network analyzers. In: Proceedings of the 44^{th} european microwave conference, Rome, Italy, pp 750–753
8. IEEE Standard 1785.1-2012 (2012) IEEE P1785: IEEE standard for rectangular metallic waveguides and their interfaces for frequencies of 110 GHz and above - Part 1: Frequency bands and waveguide dimensions
9. IEEE Standard 1785.2-2014, IEEE P1785.2: draft standard for rectangular metallic waveguides and their interfaces for frequencies of 110 GHz and above, unpublished
10. MIL-DTL-3922/67D (2009) Flanges, waveguide (contact) (round, 4 hole) (millimeter)
11. Shoaib N, Kuhlmann K, Judaschke R, Sellone M, Brunetti L (2015) Investigation of verification artifacts in WR-03 waveguides. J Infrared, Millim, Terahertz Waves 36:1089–1100
12. Shoaib N, Kuhlmann K, Judaschke R (2015) Investigation of verification artefacts in rectangular waveguides up to 325 GHz. In: 1st URSI atlantic radio science conference (URSI AT-RASC), 18–22 May 2015, pp 1-1
13. Agilent Technologies, 8493B coaxial fixed attenuator, DC to 18 GHz. http://www.keysight.com
14. Shoaib N, Kuhlmann K, Judaschke R (2015) A novel type n coaxial air-line verification standard. Metrologia 52:469–478
15. Shoaib N, Kuhlmann K, Judaschke R (2015) A novel type n coaxial air-line verification standard. In: 1st URSI atlantic radio science conference (URSI AT-RASC), 18–22 May 2015, pp 1-1
16. Taylor JR (1982) An introduction to error analysis, the study of uncertainties in physical measurements, 2nd edn. University Science Books, Sausalito, pp 209–914
17. BIPM, IEC, IFCC, ILAC, ISO, IUPAC, IUPAP and OIML (2008) JCGM 100:2008, evaluation of measurement data - Guide to the expression of uncertainty in measurement, International Organization for Standardization (ISO), (Online). http://www.bipm.org/en/publications/guides/gum.html
18. CST - Computer Simulation Technology. Information available at: http://www.cst.com
19. MATLAB - The Language of Technical Computing. Information available at: http://www.mathworks.com
20. Zeier M, Hoffmann J, Wollensack M (2012) Metas.UncLib - a measurement uncertainty calculator for advanced problems. Metrologia 49(6):809–815
21. Hall BD (2003) Calculating measurement uncertainty for complex-valued quantities. Meas Sci Technol 14(3):368–375
22. Hall BD (2002) Calculating measurement uncertainty using automatic differentiation. Meas Sci Technol 13(4):421–427
23. Hall BD (2006) Computing uncertainty with uncertain numbers. Metrologia 43(6):L56–L61
24. Ridler N (2009) Choosing line lengths for calibrating waveguide vector network analyzers at millimetre and sub-millimetre wavelengths. NPL Rep TQE 5:1–21
25. Engen GF, Hoer CA (1978) The application of "Thru-Short-Delay" to the calibration of the dual six-port. In: IEEE-MTT-S international microwave symposium digest, 27–29 June 1978, pp. 184–185
26. Ferrero A, Pisani U (1992) Two-port network analyzer calibration using an unknown thru. IEEE Microw Guided Wave Lett 2(12):505–507

General Conclusions

In this book the VNA measurements and uncertainty assessments up to submillimeter wavelengths in waveguide test-set environments are presented. The main scope is the evaluation and linear propagation of different uncertainty sources in VNA measurements. In this regard, several S-parameter measurement and uncertainty assessment comparisons are conducted. The characterization of both coaxial and waveguide standards has also been carried out.

The mathematical modelling and the measurement uncertainty evaluation for the S-parameter measurement data using an analytical approach are discussed. The measurement results for the two different waveguide sets of types WR15 and WR10, are presented The S-parameters obtained from the dimensional measurements also showed a high degree of compatibility with the measured data.

The comparison of TRL and QSOLT calibration techniques for WR10 waveguide standards demonstrated that the QSOLT can be a metrological alternative calibration technique to TRL at millimetric bands for tracing S-parameter measurements to the SI.

The flange connection repeatability investigation of the VNA in WR05 waveguide standards is based on the computation of experimental standard deviation of repeated measurements and highlighted the variability of the measured complex-valued reflection coefficient.

Finally, verification standards are analyzed for coaxial and waveguide systems. It is concluded that the custom made circular iris sections can be used as a verification standard for waveguide systems and are easier to realize than the cross-guide verification devices. For coaxial connector systems, a type N coaxial verification standard based on an air-line, with relatively simple architecture, is designed which can be used as an effective verification artefact.

N. Shoaib, *Vector Network Analyzer (VNA) Measurements and Uncertainty Assessment*, PoliTO Springer Series, DOI 10.1007/978-3-319-44772-8

Index

N. Shoaib, *Vector Network Analyzer (VNA) Measurements and Uncertainty Assessment*, PoliTO Springer Series, DOI 10.1007/978-3-319-44772-8